applied sciences

MDPI

Article

Thermodynamic and Exergoeconomic Analysis of a Supercritical CO_2 Cycle Integrated with a LiBr-H_2O Absorption Heat Pump for Combined Heat and Power Generation

Yi Yang, Zihua Wang, Qingya Ma, Yongquan Lai, Jiangfeng Wang, Pan Zhao and Yiping Dai *

School of Energy and Power Engineering, Xi'an Jiaotong University, Xi'an 710049, China; turbineyy@163.com (Y.Y.); wangzh14@stu.xjtu.edu.cn (Z.W.); xianjiaodamqy@stu.xjtu.edu.cn (Q.M.); lai546539599@stu.xjtu.edu.cn (Y.L.); jfwang@mail.xjtu.edu.cn (J.W.); panzhao@mail.xjtu.edu.cn (P.Z.)

* Correspondence: ypdai@mail.xjtu.edu.cn

Received: 5 November 2019; Accepted: 30 December 2019; Published: 1 January 2020

check for updates

Abstract: In this paper, a novel combined heat and power (CHP) system is proposed in which the waste heat from a supercritical CO_2 recompression Brayton cycle (sCO_2) is recovered by a LiBr-H_2O absorption heat pump (AHP). Thermodynamic and exergoeconomic models are established on the basis of the mass, energy, and cost balance equations. The proposed sCO_2/LiBr-H_2O AHP system is examined and compared with a stand-alone sCO_2 system, a sCO_2/DH system (sCO_2/direct heating system), and a sCO_2/ammonia-water AHP system from the viewpoints of energy, exergy, and exergoeconomics. Parametric studies are performed to reveal the influences of decision variables on the performances of these systems, and the particle swarm optimization (PSO) algorithm is utilized to optimize the system performances. Results show that the sCO_2/LiBr-H_2O AHP system can obtain an improvement of 13.39% in exergy efficiency and a reduction of 8.66% in total product unit cost compared with the stand-alone sCO_2 system. In addition, the sCO_2/LiBr-H_2O AHP system performs better than sCO_2/DH system and sCO_2/ammonia-water AHP system do, indicating that the LiBr-H_2O AHP is a preferable bottoming cycle for heat production. The detailed parametric analysis, optimization, and comparison results may provide some references in the design and operation of sCO_2/AHP system to save energy consumption and provide considerable economic benefits.

Keywords: supercritical CO_2 cycle; absorption heat pump; LiBr-H_2O solution; parametric study; optimization

1. Introduction

In the past few decades, energy crisis and environment problems became serious because of the increasing energy demand and the rapid economic development all over the world. Many efforts have been devoted into developing advanced energy conversion technologies to relieve the current challenging energy situation. For the existing energy sources (such as fossil fuels, solar, biomass, geothermal energy, and nuclear energy) and industrial waste heat sources, various novel energy conversion systems were proposed in place of the conventional ones to improve energy utilization [1]. Among these proposed systems, the supercritical CO_2 power cycle (sCO_2) is considered to be a promising technology with great potential and competiveness owing to its advantages of a compact structure, environmental friendliness and high efficiency [2–4]. The sCO_2 power cycle operates above the critical point of CO_2 (31.3 °C, 7.39 MPa). Due to the dramatic changes of thermodynamic properties near the critical point, the inlet state of its compressor is always designed just above the critical point so that the compressor work can be reduced significantly. Hence, cooling the CO_2 before compression process can be beneficial to the efficiency improvement [5–7]. However, a huge amount of heat is inevitably rejected by the cooler during the cooling process. So, it is worthwhile to reuse this low-grade heat energy through waste heat recovery systems to improve the performance of the sCO_2 cycle [8,9].

Various waste heat power generation systems were adopted to recover the waste heat of the sCO_2 cycle. Chacartegui et al. [10] applied an Organic Rankine Cycle (ORC) to reuse this waste heat for producing electric power, and compared the combined sCO_2/ORC system with two stand-alone closed CO_2 cycles. They conclu ded that the addition of ORC could improve the thermal efficiency by 7–12%. Akbari and Mahmoudi [11] conducted a thermoeconomic analysis for a combined recompression sCO_2/ORC system. Compared to the stand-alone sCO_2 cycle, the exergy efficiency increased by up to 11.7% and the total product unit cost decreased by up to 5.7% for the combined sCO_2/ORC system. Wang and Dai [12] compared a transcritical CO_2 cycle (tCO_2) with an ORC as the bottoming cycle for a recompression sCO_2 cycle. The sCO_2/tCO_2 system showed a better performance than the sCO_2/ORC system at a lower pressure ratio, while the latter had a slightly lower total product unit cost than the former. Besarati and Goswami [13] chose ORC as the bottoming cycle for a simple sCO_2 cycle, a recompression sCO_2 cycle, and a partial cooling sCO_2 cycle. It was concluded that the recompression sCO_2/ORC system presented the maximum combined cycle efficiency. Some researchers also integrated a Kalina cycle with the sCO_2 cycle to enhance the overall system performances. Li et al. [14] proposed a combined recompression sCO_2/Kalina cycle, and found out that the total product unit cost and exergy efficiency of the combined cycle were 5.5% lower and 8.02% higher than those of the sCO_2 cycle. Mahmoudi et al. [15] studied the thermodynamic and economic performances for a stand-alone sCO_2 cycle and a combined sCO_2/Kalina cycle. Results showed that combining the Kalina cycle with the sCO_2 cycle could reduce the exergy destruction significantly.

In addition to the combined power generation systems above, establishing combined power and heat/cooling systems can also enhance the overall performance for the sCO_2 cycle. In the combined power and heat/cooling systems, the low-grade waste heat of the topping cycle is transformed into cooling energy or to produce heat in bottoming cycle, which can obtain better gains than transforming high-grade electric energy into low-grade heat/cooling energy because of the lower energy conversion efficiency in the electric power generation process [16]. The absorption refrigeration cycle (ARC) is widely integrated with the sCO_2 cycle to provide electric power and cooling energy simultaneously. Wu et al. [17] investigated an combined sCO_2 cycle/ammonia-water based ARC. The thermal efficiency, exergy efficiency, and total product unit cost of the combined cycle were 26.12% and 2.73% higher, and 2.03% lower than those of the stand-alone sCO_2 cycle, respectively. Li et al. [18] coupled the lithium bromide-water ARC with a recompression sCO_2 cycle, and compared it with the recompression sCO_2 cycle/ammonia-water ARC. The single-objective optimization results showed that the sCO_2/LiBr-H_2O ARC system had a better performance than the sCO_2/ammonia-water ARC system. Recently, Balafkandeh et al. [19] developed a tri-generation system by using biomass energy based on a sCO_2 cycle and a LiBr-H_2O ARC. Compared to the sCO_2 cycle, the proposed combined cycle presented a large performance improvement in terms of efficiency and environmental impacts.

A number of studies proposed combined heat and power (CHP) systems based on sCO_2 cycle to achieve heat and electric power cogeneration. Zhang et al. [20] investigated a solar energy powered sCO_2 Rankine cycle, in which the thermal energy of recuperators was recovered by the heating water to provide heat for users directly. Moroz et al. [21] studied several types of sCO_2 cycles in a CHP plant, and compared these sCO_2 cycles with steam CHP systems. They concluded that the sCO_2 cycle should be considered as a base for future CHP plants due to its excellent performances. However, in previous sCO_2-based CHP systems, the waste heat of the sCO_2 cycle was directly supplied to heat users. The temperature of waste heat is much higher than the heating temperature of heat users, which is inconsistent with the principle of energy cascade utilization. Thus, direct heating is not a high-efficiency method to sufficiently utilize the waste heat of the sCO_2 cycle. Compared with the conventional direct heating (DH) systems, the advantage of heat amplification makes absorption heat pump (AHP) a preferable choice that can produce more heat to satisfy the user demand [22], especially when the waste heat of the sCO_2 cycle is limited or insufficient for users. However, very limited efforts were devoted to comprehensively analyzing the feasibility of AHP to recover the waste heat of the sCO_2 cycle based on the principle of energy cascade utilization. Consequently, the purpose of this study is to propose a combined sCO_2/AHP system for high-efficiency heat and power cogeneration, and to compare it with existing systems to present its advantages quantitatively.

On the other side, the most frequently used working fluids for AHP are an ammonia-water solution and a LiBr-H_2O solution. Both of them were frequently considered for comparison and discussion [23,24]. The LiBr-H_2O AHP has a smaller operational pressure and can be easier to achieve than the ammonia-water AHP. Besides, if the working fluid leaks, the water vapor in LiBr-H_2O AHP is much safer than the ammonia vapor in ammonia-water AHP. Therefore, the LiBr-H_2O AHP will be the main focus of this study while the ammonia-water AHP will be adopted as a comparison. To the best of the authors' knowledge, the LiBr-H_2O AHP has never been applied as a bottoming cycle to recover the waste heat of the sCO_2 cycle. Thus, a combined sCO_2/LiBr-H_2O AHP system is first proposed in this study as a novel high-efficiency CHP system.

In this study, a preliminary design and analysis of a CHP system is carried out, in which the topping cycle is a sCO_2 cycle driven by a nuclear reactor to generate electric power and the bottoming cycle is a LiBr-H_2O AHP to recover the waste heat of topping cycle for producing heat. Firstly, the sCO_2/LiBr-H_2O AHP system is proposed and investigated in terms of energy, exergy, and exergoeconomics. A single sCO_2 cycle, a sCO_2/DH system, and a sCO_2/ammonia-water AHP system are compared with the sCO_2/LiBr-H_2O AHP system in order to show its advantages. Then, parametric analysis is performed to reveal the influences of several key system parameters, namely the turbine inlet temperature, compressor pressure ratio, generator temperature and evaporator temperature, on the power generation, heating, and overall performances for these systems. Finally, performances of these systems are optimized and then compared by utilizing the particle swarm optimization (PSO) algorithm.

2. System Description and Assumptions

Figure 1a,b depict the schematic diagrams of the proposed sCO_2/LiBr-H_2O AHP system (supercritical CO_2 recompression Brayton cycle/LiBr-H_2O absorption heat pump system) and a sCO_2/DH system (supercritical CO_2 recompression Brayton cycle/direct heating system), respectively. In the sCO_2/DH system, a conventional direct heating system is applied to recover the waste heat in the cooler of the sCO_2 cycle. The waste heat is supplied to heat users through a direct heat exchanger (DHE). Thus, the sCO_2/DH system consists of a turbine, a main compressor (MC), a recompression compressor (RC), a high-temperature recuperator (HTR), a low-temperature recuperator (LTR), a cooler, and a DHE, as shown in Figure 1b.

The following Figure 1 shows the schematic diagrams of combined heat and power systems: (a) the sCO_2/AHP system; (b) the sCO_2/DH system.

Differently in the sCO_2/LiBr-H_2O AHP system, a part of the waste heat in the cooler is transferred to a LiBr-H_2O based AHP, so that the heat amount can be amplified to produce more heat for users, especially when the waste heat of the sCO_2 cycle is insufficient to satisfy the demand. The AHP includes a generator, an absorber, an evaporator, a condenser, a pump, and a solution heat exchanger (SHE), as shown in Figure 1a.

As both LiBr-H_2O solution and ammonia-water solution are frequently utilized as working fluids, a sCO_2/ammonia-water AHP system is established in which an ammonia-water AHP is coupled with the sCO_2 cycle, so as to conduct a comparative study with the proposed sCO_2/LiBr-H_2O AHP system. As the structure and main components are the same for both combined systems, Figure 1a also describes the sCO_2/ammonia-water AHP system.

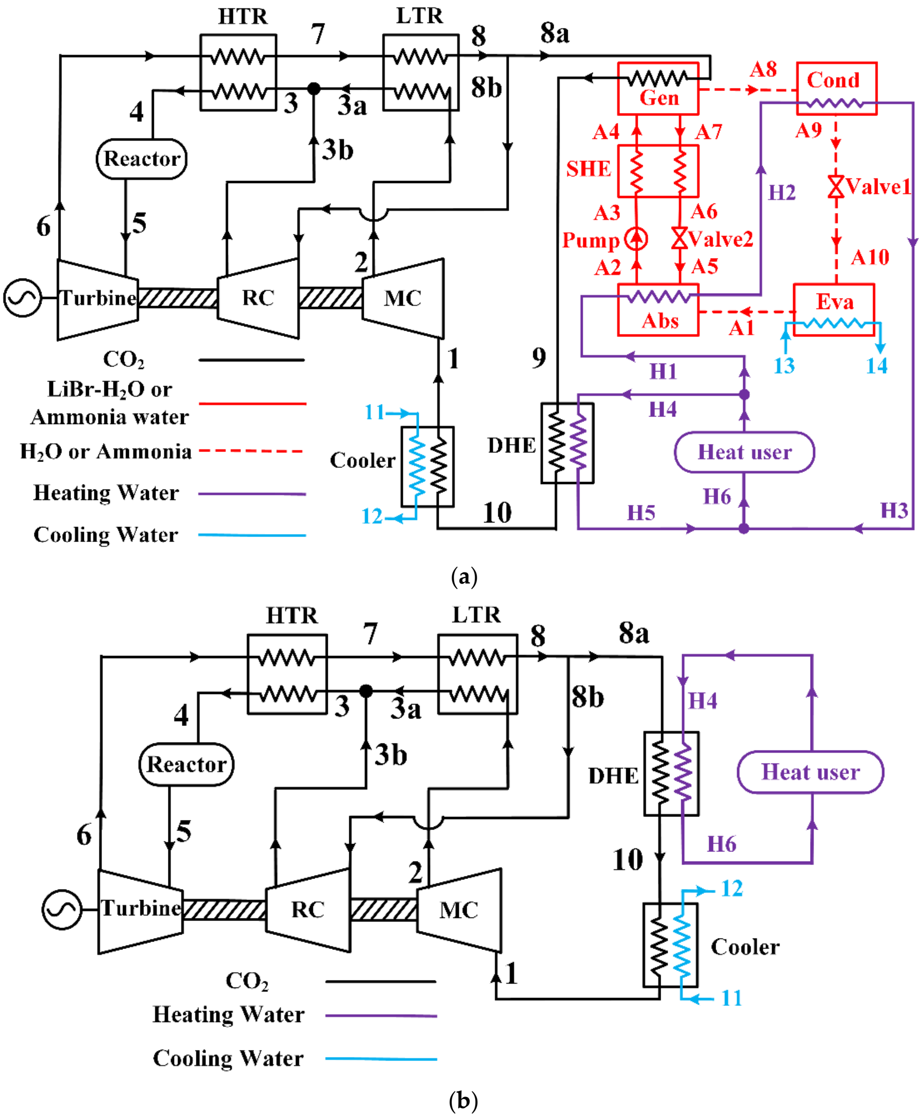

Figure 1. Schematic diagrams of combined heat and power systems: (**a**) sCO_2/AHP system; (**b**) sCO_2/DH system.

2.1. Working Process of the sCO_2/AHP System

As can be seen in Figure 1a, the sCO_2/AHP system consists of four parts. The working process for each part is introduced below,

1. sCO_2 topping cycle
    (a) The CO_2 working fluid (stream 4) absorbs heat from the reactor (stream 5) and expands in a turbine to drive an electric generator;
    (b) After expansion, the vapor exhaust (stream 6) flows into the HTR to heat stream 3, and then the outlet working fluid (stream 7) flows into the LTR to heat stream 2;
    (c) The working fluid after releasing heat (stream 8) is split into 8a and 8b;
    (d) The stream 8a releases a part of heat to drive the AHP bottoming cycle, and then (stream 9) flows into the DHE (stream 10) and the cooler before compression (stream 1) in the main compressor and afterwards (stream 2) flows into the LTR to be heated (stream 3a);
    (e) The stream 8b is compressed directly to stream 3b;
    (f) The compressed stream 3a and stream 3b are mixed to stream 3 and then heated to stream 4 before moving into the reactor.

2. AHP bottoming cycle

    (a) The diluted solution A3 (or ammonia-rich solution) absorbs heat in the SHE to state A4, and then is heated by stream 8a in the generator and separated into a strong solution A7 (or ammonia-poor solution) and a vapor stream A8;
    (b) The stream A8 is cooled to the saturated liquid (stream A9) in the condenser, throttled by the valve 1, and then heated to saturated vapor (stream A1) in the evaporator. It is noted that the heat release in the condenser is applied to reheat the heating water;
    (c) The strong solution A7 (or ammonia-poor solution) releases heat in the SHE and decompresses through the valve 2 to a low-pressure solution A5;
    (d) The strong solution A5 (or ammonia-poor solution) absorbs the vapor A1 in the absorber. The merged diluted solution (or ammonia-rich solution) is cooled by the heating water, and pressured by the pump to the high-pressure solution A3.

3. Heating water cycle

    (a) The low-temperature heating water from heat users is divided into stream H1 and stream H4;
    (b) The stream H1 obtains heat from the absorber and the condenser of AHP to state H3;
    (c) The stream H4 is heated by the CO_2 working fluid (stream 9) to state H5, then mixed with stream H3 to the high-temperature heating water H6, and finally supplied to heat users.

4. Cooling water cycle

The cooling water (stream 11) absorbs heat in the cooler (stream 12), and then a part of it (stream 13) flows into the evaporator to heat the working fluid of AHP and finally back to the cooling tower, while another part of cooling water flows back directly to the cooling tower.

2.2. Working Process of the sCO$_2$/DH System

The working process of the sCO$_2$ cycle in the sCO$_2$/DH system is same as that in Section 2.1. The only difference is that the stream 8a in Figure 1b releases heat only in the DHE, and all the heat release before the cooler is supplied to the heat users directly through the DHE.

2.3. Assumptions

The main assumptions for this study are listed as below,

(a) The systems are assumed to operate at a steady state, and the off-design performance or dynamic performance is not considered in this study;
(b) The variation of kinetic and potential energy is neglected;
(c) The pressure losses and heat losses of pipes and heat exchangers are neglected [25];
(d) Isentropic efficiencies are assumed for the turbine, pump and compressors [26];
(e) The liquid working fluid exiting the condenser (stream A9) and the generator (stream A7) is saturated liquid, while a subcooled degree of 3K is assumed at the outlet of absorber (stream A2) [27];
(f) Vapor exiting the generator is assumed to be pure ammonia for the sCO$_2$/ammonia-water AHP system [27,28];
(g) A temperature difference or an effectiveness is assumed in each heat exchanger [26].

3. System Modelings

3.1. Thermodynamic Model

The thermodynamic model for the combined cycle is developed according to the mass and energy balance equations of each component.

Thermodynamic relations and the effectiveness for HTR and LTR are expressed as Equations (1)–(4),

$$h_6 - h_7 = h_4 - h_3 \tag{1}$$

$$(h_3 - h_2)(1 - x) = h_7 - h_8 \tag{2}$$

$$\varepsilon_{HTR} = \frac{T_6 - T_7}{T_6 - T_3} \tag{3}$$

$$\varepsilon_{LTR} = \frac{T_7 - T_8}{T_7 - T_2} \tag{4}$$

where x is the mass separation ratio of stream 3b to stream 3, and ε_{HTR} and ε_{LTR} are the effectiveness of HTR and LTR, respectively.

For turbine, main compressor and recompression compressor, the isentropic efficiencies are calculated with Equation (5)–(7),

$$\eta_{\text{tur}} = \frac{h_5 - h_6}{h_5 - h_{6s}} \tag{5}$$

$$\eta_{\text{mcom}} = \frac{h_{2s} - h_1}{h_2 - h_1} \tag{6}$$

$$\eta_{\text{rcom}} = \frac{h_{3s} - h_8}{h_3 - h_8} \tag{7}$$

where η_{tur}, $\eta_{\text{mcom,}}$ and η_{rcom} are the isentropic efficiencies for the turbine, main compressor, and recompression compressor, respectively.

The thermodynamic relation for the cooler is calculated using Equation (8),

$$(1 - x)m_{\text{CO}_2}(h_{10} - h_1) = m_{cw1}(h_{12} - h_{11}) \tag{8}$$

where m_{CO2} and m_{cw1} are the mass flow rates of CO_2 and the cooling water of the cooler, respectively.

The power output of the turbine and the consumptions of two compressors can be derived as Equations (9)–(11),

$$W_{\text{tur}} = m_{\text{CO}_2}(h_5 - h_6) \tag{9}$$

$$W_{\text{mcom}} = (1 - x)m_{\text{CO}_2}(h_2 - h_1) \tag{10}$$

$$W_{\text{rcom}} = xm_{\text{CO}_2}(h_3 - h_8). \tag{11}$$

For the sCO_2/AHP system, the energy conservation equation of DHE is Equation (12),

$$Q_{\text{DHE}} = (1 - x)m_{\text{CO}_2}(h_9 - h_{10}) = m_{hw1}(h_{\text{H5}} - h_{\text{H4}}) \tag{12}$$

while that for the sCO_2/DH system is Equation (13),

$$Q_{\text{DHE}} = (1 - x)m_{\text{CO}_2}(h_8 - h_{10}) = m_{hw1}(h_{\text{H6}} - h_{\text{H4}}) \tag{13}$$

where m_{hw1} is the mass flow rate of the heating water flowing through the DHE. Q_{DHE} is the heat absorption of DHE from the topping cycle.

In the sCO_2/AHP system, the conservation equations for the AHP are expressed as follows. The thermodynamic relation for the generator is Equation (14),

$$Q_{\mathrm{Gen}} = (1-x)m_{\mathrm{CO_2}}(h_8 - h_9) = m_{\mathrm{A7}}h_{\mathrm{A7}} + m_{\mathrm{A8}}h_{\mathrm{A8}} - m_{\mathrm{A4}}h_{\mathrm{A4}} \quad (14)$$

where Q_{Gen} is the heat absorption amount of generator from the topping cycle.

Assuming y as the concentration of LiBr or ammonia in the water, the concentration balance equation is obtained as Equation (15),

$$m_{\mathrm{A4}}y_{\mathrm{A4}} = m_{\mathrm{A7}}y_{\mathrm{A7}} + m_{\mathrm{A8}}y_{\mathrm{A8}}. \quad (15)$$

The conservation equations for the condenser, evaporator, and absorber are obtained as Equations (16)–(18),

$$Q_{\mathrm{Cond}} = m_{\mathrm{A8}}h_{\mathrm{A8}} - m_{\mathrm{A9}}h_{\mathrm{A9}} = m_{hw2}(h_{\mathrm{H3}} - h_{\mathrm{H2}}) \quad (16)$$

$$Q_{\mathrm{Eva}} = m_{\mathrm{A1}}h_{\mathrm{A1}} - m_{\mathrm{A10}}h_{\mathrm{A10}} = m_{cw2}(h_{13} - h_{14}) \quad (17)$$

$$Q_{\mathrm{Abs}} = m_{\mathrm{A1}}h_{\mathrm{A1}} + m_{\mathrm{A5}}h_{\mathrm{A5}} - m_{\mathrm{A2}}h_{\mathrm{A2}} = m_{hw2}(h_{\mathrm{H2}} - h_{\mathrm{H1}}) \quad (18)$$

where m_{hw2} is the mass flow rate of the heating water flowing through the AHP.

The conservation equation for SHE is obtained as Equation (19),

$$m_{\mathrm{A4}}h_{\mathrm{A4}} - m_{\mathrm{A3}}h_{\mathrm{A3}} = m_{\mathrm{A7}}h_{\mathrm{A7}} - m_{\mathrm{A6}}h_{\mathrm{A6}}. \quad (19)$$

For the pump, the isentropic efficiency and power consumption are defined according Equations (20) and (21),

$$\eta_{\mathrm{pump}} = \frac{h_{\mathrm{A3}s} - h_{\mathrm{A2}}}{h_{\mathrm{A3}} - h_{\mathrm{A2}}} \quad (20)$$

$$W_{\mathrm{pump}} = m_{\mathrm{A3}}h_{\mathrm{A3}} - m_{\mathrm{A2}}h_{\mathrm{A2}}. \quad (21)$$

The net output power of the combined cycle can be calculated as Equation (22),

$$W_{\mathrm{net}} = W_{\mathrm{tur}} - W_{\mathrm{rcom}} - W_{\mathrm{mcom}} - W_{\mathrm{pump}}. \quad (22)$$

The heat amount supplied to the heat users, $Q_{h,users}$, and the heat absorption from the topping cycle for the purpose of heating, $Q_{h,absorb}$ were then defined for both combined systems. For the sCO_2/DH system, they are expressed as Equations (23) and (24),

$$Q_{h,users} = m_{hw1}(h_{\mathrm{H6}} - h_{\mathrm{H4}}) \quad (23)$$

$$Q_{h,absorb} = (1-x)m_{\mathrm{CO_2}}(h_8 - h_{10}). \quad (24)$$

For the sCO_2/AHP system, they are expressed as Equations (25) and (26),

$$Q_{h,users} = (m_{hw1} + m_{hw2})(h_{\mathrm{H6}} - h_{\mathrm{H1}}) \quad (25)$$

$$Q_{h,absorb} = Q_{\mathrm{Gen}} + (1-x)m_{\mathrm{CO_2}}(h_9 - h_{10}). \quad (26)$$

Ignoring the variations in kinetic and potential exergies, the exergy of a stream consists of two parts, namely the chemical and physical exergy, as Equation (27),

$$E = E_{\mathrm{ph}} + E_{\mathrm{ch}}. \quad (27)$$

The physical exergy can be calculated with Equation (28),

$$E_{\mathrm{ph}} = m[(h - h_0) - T_0(s - s_0)]. \quad (28)$$

For the ammonia water in AHP, the chemical exergy can be determined with Equation (29) [29,30],

$$E_{\mathrm{ph}} = m\left[\left(\frac{y}{M_{\mathrm{NH_3}}}\right)e^0_{\mathrm{ch,NH_3}} + \left(\frac{1-y}{M_{\mathrm{H_2O}}}\right)e^0_{\mathrm{ch,H_2O}}\right] \tag{29}$$

where $e^0_{\mathrm{ch,NH_3}}$ and $e^0_{\mathrm{ch,H_2O}}$ are the standard chemical exergies of ammonia and water, respectively. For the LiBr-H_2O solution, the chemical exergy can be calculated according to reference [31].

Then, the exergy balance equation for each component in the combined systems can be obtained, as shown in Table 1. On this basis, the total exergy destruction of the combined system is expressed as Equation (30),

$$I_{\mathrm{total}} = \sum I_{\mathrm{components}}. \tag{30}$$

The following Table 1 shows the exergy balance equations for sCO_2/AHP system and sCO_2/DH system.

Table 1. Exergy balance equations for the sCO_2/AHP system and sCO_2/DH system.

System Components	sCO_2/AHP System	sCO_2/DH System
reactor	$E_{\mathrm{core}} + E_4 = E_5 + I_{\mathrm{core}}$	$E_{\mathrm{core}} + E_4 = E_5 + I_{\mathrm{core}}$
sCO_2 turbine	$E_5 = E_6 + W_{\mathrm{tur}} + I_{\mathrm{tur}}$	$E_5 = E_6 + W_{\mathrm{tur}} + I_{\mathrm{tur}}$
HTR	$E_3 + E_6 = E_4 + E_7 + I_{\mathrm{HTR}}$	$E_3 + E_6 = E_4 + E_7 + I_{\mathrm{HTR}}$
LTR	$E_2 + E_7 = E_{3a} + E_8 + I_{\mathrm{LTR}}$	$E_2 + E_7 = E_{3a} + E_8 + I_{\mathrm{LTR}}$
main compressor	$E_1 + W_{\mathrm{mcom}} = E_2 + I_{\mathrm{mcom}}$	$E_1 + W_{\mathrm{mcom}} = E_2 + I_{\mathrm{mcom}}$
recompression compressor	$E_{8b} + W_{\mathrm{rcom}} = E_{3b} + I_{\mathrm{rcom}}$	$E_{8b} + W_{\mathrm{rcom}} = E_{3b} + I_{\mathrm{rcom}}$
cooler	$E_{10} = E_1 + I_{\mathrm{cooler}}$	$E_{10} = E_1 + I_{\mathrm{cooler}}$
DHE	$E_9 + E_{\mathrm{H4}} = E_{10} + E_{\mathrm{H5}} + I_{\mathrm{DHE}}$	$E_{8a} + E_{\mathrm{H4}} = E_{10} + E_{\mathrm{H6}} + I_{\mathrm{DHE}}$
generator	$E_{8a} + E_{\mathrm{A4}} = E_9 + E_{\mathrm{A7}} + E_{\mathrm{A8}} + I_{\mathrm{Gen}}$	/
absorber	$E_{\mathrm{A1}} + E_{\mathrm{A5}} + E_{\mathrm{H1}} = E_{\mathrm{A2}} + E_{\mathrm{H2}} + I_{\mathrm{Abs}}$	/
SHE	$E_{\mathrm{A3}} + E_{\mathrm{A7}} = E_{\mathrm{A4}} + E_{\mathrm{A6}} + I_{\mathrm{SHE}}$	/
condenser	$E_{\mathrm{A8}} + E_{\mathrm{H2}} = E_{\mathrm{A9}} + E_{\mathrm{H3}} + I_{\mathrm{Cond}}$	/
Evaporator	$E_{\mathrm{A10}} + E_{13} = E_{\mathrm{A1}} + E_{14} + I_{\mathrm{Eva}}$	/
Pump	$E_{\mathrm{A2}} + W_{\mathrm{pump}} = E_{\mathrm{A3}} + I_{\mathrm{pump}}$	/
Valve1	$E_{\mathrm{A9}} = E_{\mathrm{A10}} + I_{\mathrm{Valve1}}$	/
Valve2	$E_{\mathrm{A6}} = E_{\mathrm{A5}} + I_{\mathrm{Valve2}}$	/

3.2. Exergoeconomic Model

On the basis of the mass, energy and exergy balances above, the exergoeconomic analysis can be conducted to obtain the cost per unit exergy of product streams and to assess the combined systems. Firstly, all energy and exergy values should be determined, which has been achieved in the above section. Then, the fuel-production definition for the energy conversion system should be determined. For the sCO_2/AHP system and sCO_2/DH system in this study, the definitions are shown in Table 2. Finally, the cost balance equations can be constructed for all components. For the kth system component, the cost balance can be expressed with Equations (31)–(34) [32,33],

$$\sum \dot{C}_{out,k} + \dot{C}_{w,k} = \sum \dot{C}_{in,k} + \dot{C}_{q,k} + \dot{Z}_k \tag{31}$$

in which,

$$\dot{C} = c \cdot E \tag{32}$$

$$\dot{C}_{q,k} = c_{q,k} \cdot E_{q,k} \tag{33}$$

$$\dot{C}_{w,k} = c_{w,k} \cdot W \tag{34}$$

where $\dot{C}$ is the cost rate of the stream, while $\dot{C}_q$ and $\dot{C}_w$ are the cost rate of the heat transfer and power, respectively. $\dot{Z}_k$ represents the total cost rate of capital investment, operation and maintenance, which can be obtained as Equation (35),

$$\dot{Z}_k = \dot{Z}_k^{CI} + \dot{Z}_k^{OM}. \quad (35)$$

where $\dot{Z}_k^{CI}$ denotes the annual levelized capital investment and $\dot{Z}_k^{OM}$ denotes the annual levelized operation and maintenance cost. They can be obtained with Equations (36) and (37) [32],

$$\dot{Z}_k^{OM} = \gamma_k Z_k / \tau \quad (36)$$

$$\dot{Z}_k^{CI} = \left(\frac{CRF}{\tau}\right) Z_k \quad (37)$$

where CRF, τ and γ represent the capital recovery factor, operating hours, and the maintenance factor, respectively. CRF is relative to the bank interest rate, which can be expressed as Equation (38),

$$CRF = \frac{i_r(1+i_r)^n}{(1+i_r)^n - 1} \quad (38)$$

where i_r is the interest rate, and n is the number of operation years. The values of i_r, n, τ, γ, and the expression of cost function Z_k for each component in this study are listed in Table 3.

The following Table 2 shows the fuel-product definitions for the combined systems.

Table 2. Fuel-product definitions for the combined systems.

Components	sCO$_2$/AHP System		sCO$_2$/DH System	
	Fuel Exergy	**Product Exergy**	**Fuel Exergy**	**Product Exergy**
Reactor	$E_4 + E_{in}$	E_5	$E_4 + E_{in}$	E_5
sCO$_2$ turbine	$E_5 - E_6$	W_{tur}	$E_5 - E_6$	W_{tur}
HTR	$E_6 - E_7$	$E_4 - E_3$	$E_6 - E_7$	$E_4 - E_3$
LTR	$E_7 - E_8$	$E_{3a} - E_2$	$E_7 - E_8$	$E_{3a} - E_2$
Main compressor	W_{mcom}	$E_2 - E_1$	W_{mcom}	$E_2 - E_1$
Recompression compressor	W_{rcom}	$E_{3b} - E_{8b}$	W_{rcom}	$E_{3b} - E_{8b}$
Cooler	$E_{10} - E_1$	$E_{12} - E_{11}$	$E_{10} - E_1$	$E_{12} - E_{11}$
DHE	$E_9 - E_{10}$	$E_{H5} - E_{H4}$	$E_{8a} - E_{10}$	$E_{H6} - E_{H4}$
Generator	$E_{8a} - E_9$	$E_{A7} + E_{A8} - E_{A4}$	/	/
Absorber	$E_{A1} + E_{A5} - E_{A2}$	$E_{H2} - E_{H1}$	/	/
Condenser	$E_{A8} - E_{A9}$	$E_{H3} - E_{H2}$	/	/
Evaporator	$E_{13} - E_{14}$	$E_{A1} - E_{A10}$	/	/
SHX	$E_{A7} - E_{A6}$	$E_{A4} - E_{A3}$	/	/
Pump	W_{pump}	$E_{A3} - E_{A2}$	/	/
Valve1	E_{A9}	E_{A10}	/	/
Valve2	E_{A6}	E_{A5}	/	/

Table 3 shows the cost functions of the system components.

Table 3. Cost functions of the system components [11,32,34].

Component	Economic Parameters
Number of operation year (n)	20
Annual operation hours (τ)	8000
Interest rate (i_r)	0.12
Maintenance factor (γ)	0.06
Reactor	$Z_{\text{core}} = C_1 * Q_{\text{core}},\ C_1 = 283\$/\text{kW}_{\text{th}}$
sCO_2 turbine	$Z_{\text{tur}} = 479.34 \times m_{\text{in}}\left(\frac{1}{0.93-\eta_{\text{tur}}}\right) \times \ln(PRc) \times \left(1 + e^{(0.036T_{\text{in}}-54.4)}\right)$
Compressor	$Z_{\text{mcom\&rcom}} = 71.1 \times m_{\text{in}}\left(\frac{1}{0.92-\eta_{\text{mcom\&rcom}}}\right) \times PRc \times \ln(PRc)$
HTR, LTR, Cooler, DHE	$Z_k = 30 \times \text{Mass}_k$
Generator, Absorber, SHE, Condenser, Evaporator	$Z_k = Z_{\text{ref}}\left(\frac{A_k}{A_{\text{ref}}}\right)^{0.6}$
Pump	$Z_{\text{pump}} = 1120 \times W_{\text{pump}}^{0.8}$

The mass and areas of heat exchangers in Table 3 are determined based on the heat exchanger design according to the mathematical models of different heat exchanger types. Compared to the conventional shell-and-tube heat exchanger, the Print Circuit Heat Exchanger (PCHE) shows higher heat transfer performances with a larger operation range (up to 980 °C and 96.5 MPa), which has been widely suggested and evaluated in previous studies [35–37]. Thus, PCHE is chosen as the heat exchangers (HTR, LTR, DHE, and cooler) in the SCO_2 topping cycle. Corresponding mathematical models for PCHE are established according some typical investigations [38,39], as listed in Table 4. Unlike in the SCO_2 topping cycle, the pressure and temperature in the AHP bottoming cycle are much lower, so that traditional high-efficiency heat exchangers are adopted in AHP for the generator, absorber, condenser, evaporator, and SHE. Table 4 describes the heat exchanger types and corresponding mathematical models for AHP cycles with both LiBr-H_2O solution and ammonia water. With these mathematical models, the heat exchange areas for all heat exchangers are calculated by using the enhanced logarithmic mean temperature difference method [40].

The following Table 4 shows the mathematical models for heat exchangers.

Table 4. Mathematical models for heat exchangers.

Components	Types	Fluids	Mathematical Models
HTR, LTR, DHE, cooler	PCHE	CO_2	Gnielinski expression [a]
Generator	Nucleate pool boiling heat exchanger	CO_2 LiBr-H_2O Ammonia water	Gnielinski expression [a] Jakob and Hawkin expression [b] Táboas's correlation [c]
Evaporator	Horizontal falling film heat exchanger	Cooling water Water (H_2O) Ammonia	Petukhov-Popov expression [d] Wilke's correlation [e] Lee expression [f]
Condenser	Horizontal tubes heat exchanger	Heating water Vapor	Petukhov-Popov expression [d] Nusselt expression [g]
Absorber	Horizontal falling film heat exchanger	LiBr-H_2O Ammonia water Heating water	Wilke's correlation [e] Lee expression [f] Petukhov-Popov expression [d]
SHE	Annular heat exchanger	Ammonia water or LiBr-H_2O	Gnielinski expression [a]

[a] Gnielinski expression [38]; [b] Jakob and Hawkin expression [41]; [c] Táboas's correlation [42]; [d] Petukhov-Popov expression [43]; [e] Wilke's correlation [44]; [f] Lee expression [45]; [g] Nusselt expression [46].

Finally, Table 5 lists the cost balance equations for sCO_2/AHP system and sCO_2/DH system with auxiliary equations. The cost rate of cooling water is assumed to be zero as it is generally regarded as a free resource. The electric power consumed by the pump in the AHP is assumed to come from the power production of the turbine. In addition, the capital investment cost at the present year is obtained according to the cost indices, namely the Chemical Engineering Plant Cost Index (CEPCI). The cost at present year can be obtained with Equation (39) [32],

$$\text{Cost at present year} = \text{Original cost} \times \frac{\text{Cost index for present year}}{\text{Cost index for original year}}. \quad (39)$$

The Gauss-Seidel method is utilized to solve the linear system of equations in the Table 5 for two combined systems. After the solution, the cost rates for all exergy streams can be obtained.

Table 5 shows the cost balance equations and auxiliary equations for the combined systems.

Table 5. Cost balance equations and auxiliary equations for the combined systems.

Components	sCO_2/DH System	sCO_2/AHP System
Reactor	$\dot{C}_5 = \dot{C}_4 + \dot{Z}_{reactor} + \dot{C}_{fuel}$	$\dot{C}_5 = \dot{C}_4 + \dot{Z}_{reactor} + \dot{C}_{fuel}$
sCO_2 turbine	$\dot{C}_6 + \dot{C}_{W_{tur}} = \dot{C}_5 + \dot{Z}_{tur}$ $\frac{\dot{C}_5}{\dot{E}_5} = \frac{\dot{C}_6}{\dot{E}_6}$	$\dot{C}_6 + \dot{C}_{W_{tur}} = \dot{C}_5 + \dot{Z}_{tur}$ $\frac{\dot{C}_5}{\dot{E}_5} = \frac{\dot{C}_6}{\dot{E}_6}$
HTR	$\dot{C}_4 + \dot{C}_7 = \dot{C}_3 + \dot{C}_6 + \dot{Z}_{HTR}$ $\frac{\dot{C}_6}{\dot{E}_6} = \frac{\dot{C}_7}{\dot{E}_7}, \dot{C}_3 = \dot{C}_{3a} + \dot{C}_{3b}$	$\dot{C}_4 + \dot{C}_7 = \dot{C}_3 + \dot{C}_6 + \dot{Z}_{HTR}$ $\frac{\dot{C}_6}{\dot{E}_6} = \frac{\dot{C}_7}{\dot{E}_7}, \dot{C}_3 = \dot{C}_{3a} + \dot{C}_{3b}$
LTR	$\dot{C}_8 + \dot{C}_{3a} = \dot{C}_2 + \dot{C}_7 + \dot{Z}_{LTR}$ $\frac{\dot{C}_7}{\dot{E}_7} = \frac{\dot{C}_8}{\dot{E}_8}, \dot{C}_{8a} = \dot{C}_8(1-x)$	$\dot{C}_8 + \dot{C}_{3a} = \dot{C}_2 + \dot{C}_7 + \dot{Z}_{LTR}$ $\frac{\dot{C}_7}{\dot{E}_7} = \frac{\dot{C}_8}{\dot{E}_8}, \dot{C}_{8a} = \dot{C}_8(1-x)$
Main compressor	$\dot{C}_2 = \dot{C}_1 + \dot{C}_{W_{mcom}} + \dot{Z}_{mcom}$ $\frac{\dot{C}_{W_{mcom}}}{\dot{W}_{mcom}} = \frac{\dot{C}_{W_{tur}}}{\dot{W}_{tur}}$	$\dot{C}_2 = \dot{C}_1 + \dot{C}_{W_{mcom}} + \dot{Z}_{mcom}$ $\frac{\dot{C}_{W_{mcom}}}{\dot{W}_{mcom}} = \frac{\dot{C}_{W_{tur}}}{\dot{W}_{tur}}$
Recompression compressor	$\dot{C}_{3b} = \dot{C}_{8b} + \dot{C}_{W_{rcom}} + \dot{Z}_{rcom}$ $\frac{\dot{C}_{W_{rcom}}}{\dot{W}_{rcom}} = \frac{\dot{C}_{W_{tur}}}{\dot{W}_{tur}}, \dot{C}_{8b} = x\dot{C}_8$	$\dot{C}_{3b} = \dot{C}_{8b} + \dot{C}_{W_{rcom}} + \dot{Z}_{rcom}$ $\frac{\dot{C}_{W_{rcom}}}{\dot{W}_{rcom}} = \frac{\dot{C}_{W_{tur}}}{\dot{W}_{tur}}, \dot{C}_{8b} = x\dot{C}_8$
DHE	$\dot{C}_{10} + \dot{C}_{H6} = \dot{C}_{8a} + \dot{C}_{H4} + \dot{Z}_{DHE}$ $\frac{\dot{C}_{8a}}{\dot{E}_{8a}} = \frac{\dot{C}_{10}}{\dot{E}_{10}}$	$\dot{C}_{10} + \dot{C}_{H5} = \dot{C}_9 + \dot{C}_{H4} + \dot{Z}_{DHE}$ $\frac{\dot{C}_9}{\dot{E}_9} = \frac{\dot{C}_{10}}{\dot{E}_{10}}, \dot{C}_{H6} = \dot{C}_{H5} + \dot{C}_{H3}$
Cooler	$\dot{C}_1 + \dot{C}_{12} = \dot{C}_{10} + \dot{C}_{11} + \dot{Z}_{cooler}$ $\dot{C}_{11} = 0, \dot{C}_{12} = 0$	$\dot{C}_1 + \dot{C}_{12} = \dot{C}_{10} + \dot{C}_{11} + \dot{Z}_{cooler}$ $\dot{C}_{11} = 0, \dot{C}_{12} = 0$
Generator	/	$\dot{C}_{A7} + \dot{C}_{A8} + \dot{C}_9 =$ $\dot{C}_{A4} + \dot{C}_{8a} + \dot{Z}_{Gen}$ $\frac{\dot{C}_{8a}}{\dot{E}_{8a}} = \frac{\dot{C}_9}{\dot{E}_9}, \frac{\dot{C}_{A7}-\dot{C}_{A4}}{\dot{E}_{A7}-\dot{E}_{A4}} = \frac{\dot{C}_{A8}-\dot{C}_{A4}}{\dot{E}_{A8}-\dot{E}_{A4}}$
Condenser	/	$\dot{C}_{A9} + \dot{C}_{H3} = \dot{C}_{A8} + \dot{C}_{H2} + \dot{Z}_{Cond}$ $\frac{\dot{C}_{A8}}{\dot{E}_{A8}} = \frac{\dot{C}_{A9}}{\dot{E}_{A9}}$
Evaporator	/	$\dot{C}_{A1} + \dot{C}_{14} = \dot{C}_{A10} + \dot{C}_{13} + \dot{Z}_{Eva}$ $\dot{C}_{13} = 0, \dot{C}_{14} = 0$
Absorber	/	$\dot{C}_{A2} + \dot{C}_{H2} =$ $\dot{C}_{A1} + \dot{C}_{A5} + \dot{C}_{H1} + \dot{Z}_{Abs}$ $\frac{\dot{C}_{A1}+\dot{C}_{A5}}{\dot{E}_{A1}+\dot{E}_{A5}} = \frac{\dot{C}_{A2}}{\dot{E}_{A2}}, \frac{\dot{C}_{H1}}{\dot{E}_{H1}} = \frac{\dot{C}_{H4}}{\dot{E}_{H4}}$
SHE	/	$\dot{C}_{A4} + \dot{C}_{A6} = \dot{C}_{A3} + \dot{C}_{A7} + \dot{Z}_{SHE}$ $\frac{\dot{C}_{A6}}{\dot{E}_{A6}} = \frac{\dot{C}_{A7}}{\dot{E}_{A7}}$
Pump	/	$\dot{C}_{A3} = \dot{C}_{A2} + \dot{C}_{W_{pump}} + \dot{Z}_{pump}$ $\frac{\dot{C}_{W_{pump}}}{\dot{W}_{pump}} = \frac{\dot{C}_{W_{tur}}}{\dot{W}_{tur}}$

3.3. Performance Evaluation

In order to evaluate the performances of the proposed sCO_2/AHP system and the sCO_2/DH system, several criterions are considered in this study, including the coefficient of power performance (*COPP*), coefficient of heat performance (*COHP*), overall system exergy efficiency (η_{ex}) and total product unit cost (c_{total}). The *COPP* and *COHP* represent the electric power generation and heat production capacity, respectively, which are defined according to Equations (40) and (41) [18,47],

$$COPP = \frac{W_{net}}{Q_{core}} \tag{40}$$

$$COHP = \frac{Q_{h,users}}{Q_{h,absorb}} \tag{41}$$

where $Q_{h,users}$ is the heat amount supplied to the heat users, while $Q_{h,absorb}$ is the heat absorption from the topping cycle for the purpose of heating. The definitions of $Q_{h,users}$ and $Q_{h,absorb}$ can be found in Equations (23)–(26).

The exergy efficiency η_{ex} can be defined by Equations (42)–(44) [32,47],

$$\eta_{ex} = \frac{W_{net} + E_{h,users}}{E_{core}}. \tag{42}$$

$E_{h,users}$ is the exergy that heat users obtain from the DHE and AHP. For the sCO_2/DH system,

$$E_{h,users} = E_{H6} - E_{H4} \tag{43}$$

while for the sCO_2/AHP system,

$$E_{h,users} = E_{H6} - E_{H4} - E_{H1}. \tag{44}$$

The total product unit cost c_{total} presents the system performance in terms of economics, which is determined by Equation (45) [32],

$$c_{total} = \frac{\sum_{i=1}^{n_k} \dot{Z}_k + \sum_{i=1}^{n_f} c_{fi} E_{fi}}{\sum_{i=1}^{n_p} E_{pi}} \tag{45}$$

where E_{fi} and E_{pi} are the exergy flow rate of the fuel and the product, respectively. n_k, n_f, and n_p represent the number of components, fuel components, and product components.

4. Model Verifications

In this section, model verifications are conducted to ensure the reliability and accuracy of the thermodynamic models for the following performance evaluation and analysis. The results of present model are compared to the reported data in published studies under the same conditions. As the overall system proposed in this study contains two parts: a recompression sCO_2 topping cycle and an AHP bottoming cycle, both of them should be validated. In addition, the verification of the AHP bottoming cycle is carried out for both LiBr-H_2O solution and ammonia water.

By using the software Matlab, the thermodynamic and exergoeconomic simulation platform is constructed according to the mass, energy, and cost balance equations in Section 3 to simulate the system performances under different conditions. Besides, the software REFPROP NIST is combined with Matlab to evaluate the physical and thermodynamic properties of CO_2, water, ammonia, and ammonia-water solution, but those of the LiBr-H_2O solution are not included. Therefore, according to Pátek and Klomfar [48], a set of empirical formulas are utilized to calculate the pressure, enthalpy, entropy, density, and isobaric heat capacity of LiBr-H_2O solution in the temperature range of 273–500 K and the concentration range of 0–75 wt%. As the crystallization of LiBr-H_2O solution should be avoided during the system operation, the solubility curve of pure LiBr in water by Boryta [49] is utilized to examine whether the crystallization occurs for all LiBr-H_2O streams. These formulas and methods cover the application range of LiBr-H_2O solution in this study and provide a solid foundation for the following analysis.

4.1. Verification of Recompression sCO_2 Cycle Model

The first verification is conducted by comparing the results of the recompression sCO_2 cycle with the reported data by Sarkar and Bhattacharyya [6] under the same conditions to validate the sCO_2 topping cycle model, as shown in Table 6. Clearly, the simulated results of the present model show an excellent agreement with the published results. Thus, the developed thermodynamic model for the sCO_2 cycle is accurate and reliable enough to be applied for the following investigation and analysis.

Table 6 shows the comparison between the simulated results and the published data for the sCO_2 cycle.

Table 6. Comparison between the simulated results and the published data for the sCO_2 cycle.

Parameters				x		η_{th}	
T_{min} (°C)	T_{max} (°C)	P_{max} (MPa)	*PRc*	Present	Published	Present	Published
32	550	20	2.64	0.3332	0.334	41.18	41.18
32	550	30	3.86	0.3546	0.355	43.32	43.32
32	750	20	2.65	0.2212	0.223	46.07	46.07
32	750	30	3.94	0.2809	0.281	49.84	49.83
50	550	20	2.40	0.1842	0.184	36.71	36.71
50	550	30	2.80	0.2533	0.254	38.94	38.93
50	750	20	2.88	0.0962	0.109	43.50	43.50
50	750	30	3.08	0.1745	0.175	45.28	45.28

4.2. Verification of LiBr-H_2O AHP Model

Then the AHP model using LiBr-H_2O solution is examined. Cheng and Shih [47] conducted a detailed thermodynamic analysis for a LiBr-H_2O AHP and reported the main thermodynamic state points, as listed in Table 7. By setting the same thermodynamic conditions with those in Reference [47], the simulated results are obtained based on the present AHP model, and also listed in Table 7 for comparison. In addition, the calculated *COHP* is 1.695 here while the reported *COHP* is 1.69. Obviously, the results of present model match reasonably with the published data, which proves the accuracy of the LiBr-H_2O AHP model in this study.

The following Table 7 shows the comparison between the simulated results and the published data for LiBr-H_2O AHP.

Table 7. Comparison between the simulated results and the published data for LiBr-H_2O AHP.

State Points	T (°C)		h (kJ/kg)	
	Present	Published	Present	Published
A7	164.85	162.75	369.49	365.80
A4	142.63	140.76	313.86	310.30
A2	91.99	92.94	216.03	217.87
A6	106.75	106.90	280.22	265.63
A8	160.52	162.75	2798.07	2797.36
A1	51.85	51.85	2594.55	2595.19
A9	96.85	96.85	405.88	404.90

4.3. Verification of Ammonia-Water AHP Model

Finally, the ammonia-water AHP model is validated by using the reported results in Wang and Ferreira's work [50]. The same assumptions and conditions are adopted in the simulation platform:

(1) The temperatures of generator, condenser, absorber and evaporator are set to be 120 °C, 45 °C, 45 °C, and 10 °C; (2) The minimum temperature approach of SHE is set to be 5 K; (3) The solution leaving the absorber is assumed to have a subcooling of 3 K. Then, the comparison is shown in Table 8, which indicates a high agreement between two groups of results.

Table 8 shows the comparison between the simulated results and the published data for ammonia-water based AHP.

Table 8. Comparison between the simulated results and the published data for ammonia-water based AHP.

Parameters	Present Results	Published Results
y_{A2}	0.481	0.481
y_{A7}	0.335	0.335
q_{A4}	0.023	0.024
circulation ratio	4.554	4.555
COHP	1.615	1.612

5. Results and Discussions

In this section, the energy, exergy, and economic performances of the proposed sCO_2/LiBr-H_2O AHP system are analyzed. Performance comparisons are conducted between the sCO_2/LiBr-H_2O AHP system with a single sCO_2 system, a sCO_2/DH system, and a sCO_2/ammonia-water AHP system. Parametric studies are carried out to find out the influences of some key parameters on the system performance indicators, including *COPP*, *COHP*, η_{ex}, and c_{total}, as defined in Section 3.3. Then, the particle swarm optimization (PSO) algorithm is adopted to obtain the system optimal operation conditions.

The main input parameters and assumptions are listed in Table 9. By using these input conditions, the parameters of system state points are calculated and summarized in Tables 10–12 for the sCO_2/LiBr-H_2O AHP system, sCO_2/ammonia-water AHP system and sCO_2/DH system, respectively.

The following Table 9 shows the main input conditions for the simulation.

Table 9. The main input conditions for the simulation.

Items	Values
T_0 (°C)	25
P_0 (MPa)	0.101325
Q_{core} (MW)	600 [a]
T_{core} (°C)	800 [a]
T_1 (°C)	35 [a]
P_1 (MPa)	7.4 [a]
η_{mcom} & η_{rcom}	0.85 [b]
η_{tur}	0.86 [c]
η_{pump}	0.75 [d]
ε_{HTR} & ε_{LTR}	0.86 [b]
$\Delta T_{DHE,end}$ (°C)	5 [d]
$\Delta T_{SHE,end}$ (°C)	5 [d]
T_{H6} (°C)	60 [e]
T_{H1} (°C)	45 [e]
P_{user} (MPa)	1.0 [e]
Fuel cost ($/MWh)	7.4 [a]

[a] Reference [11]; [b] reference [51]; [c] reference [52]; [d] reference [50]; [e] reference [53].

Table 10 shows the thermodynamic properties and costs of exergy streams for the sCO_2/LiBr-H_2O AHP system.

Table 10. Thermodynamic properties and costs of exergy streams for the sCO_2/LiBr-H_2O AHP system.

State Points	T (°C)	P (MPa)	h (kJ/kg)	s (kJ/(kg·K))	m (kg/s)	e_{ph} (kJ/kg)	e_{ch} (kJ/kg)	$\dot{C}$ ($/h)	c ($/GJ)
1	35.00	7.40	402.40	1.663	2309.66	216.60	/	26,077.65	14.480
2	110.06	20.72	444.87	1.680	2309.66	254.09	/	33,328.11	15.775
3	245.43	20.72	656.60	2.159	3099.68	322.95	/	57,628.04	15.991
4	393.02	20.72	841.06	2.473	3099.68	413.97	/	73,239.23	15.855
5	550.00	20.72	1034.63	2.734	3099.68	529.77	/	84,301.17	14.260
6	433.11	7.40	906.74	2.763	3099.68	392.97	/	62,533.52	14.260
7	271.71	7.40	722.28	2.467	3099.68	296.85	/	47,237.39	14.260
8	132.69	7.40	564.63	2.133	3099.68	238.91	/	38,017.79	14.260
9	106.60	7.40	532.82	2.052	2309.66	231.26	/	27,421.47	14.260
10	50.00	7.40	447.38	1.806	2309.66	218.94	/	25,959.82	14.260
11	25.00	0.1013	104.92	0.367	2485.38	0.00	/	0.00	0.000
12	35.00	0.1013	146.72	0.505	2485.38	0.69	/	0.00	0.000
13	35.00	0.1013	146.72	0.505	2287.10	0.69	/	0.00	0.000
14	29.00	0.1013	121.64	0.423	2287.10	0.11	/	0.00	0.000
A1	26.00	0.0034	2548.32	8.535	24.74	8.06	478.83	477.82	11.017
A2	55.00	0.0034	119.31	0.353	157.07	2.92	490.90	3252.42	11.648
A3	55.00	0.0158	119.31	0.353	157.07	2.92	490.90	3252.71	11.649
A4	91.60	0.0158	197.37	0.578	157.07	13.76	509.19	3462.53	11.710
A5	60.00	0.0034	190.79	0.387	132.32	3.41	628.81	3535.42	11.739
A6	60.00	0.0158	190.79	0.386	132.32	3.42	628.81	3535.42	11.739
A7	110.00	0.0158	283.45	0.646	132.32	18.84	649.17	3735.49	11.739
A8	110.00	0.0158	2705.90	8.288	24.74	239.39	478.83	653.86	10.221
A9	55.00	0.0158	230.26	0.768	24.74	5.83	478.83	441.23	10.221
A10	26.00	0.0034	230.26	0.787	24.74	0.31	478.83	441.23	10.338
H1	45.00	1.00	189.30	0.638	3329.79	3.58	/	0.00	0.000
H2	50.00	1.00	210.19	0.703	3329.79	5.05	/	803.80	13.280
H3	54.40	1.00	228.59	0.760	3329.79	6.59	/	1030.05	13.045
H4	45.00	1.00	189.30	0.638	1903.60	3.58	/	0.00	0.000
H5	69.79	1.00	292.97	0.952	1903.60	13.70	/	1726.18	18.385
H6	60.00	1.00	252.00	0.831	5233.39	8.87	/	2756.23	16.495

Table 11 shows the thermodynamic properties and costs of exergy streams for the sCO_2/ammonia-water AHP system.

Table 11. Thermodynamic properties and costs of exergy streams for the sCO_2/ammonia-water AHP system.

State Points	T (°C)	P (MPa)	h (kJ/kg)	s (kJ/(kg·K))	m (kg/s)	e_{ph} (kJ/kg)	e_{ch} (kJ/kg)	$\dot{C}$ ($/h)	c ($/GJ)
1	35.00	7.40	402.40	1.663	2309.66	216.60	/	26,077.65	14.480
2	110.06	20.72	444.87	1.680	2309.66	254.09	/	33,328.11	15.775
3	245.43	20.72	656.60	2.159	3099.68	322.95	/	57,628.04	15.991
4	393.02	20.72	841.06	2.473	3099.68	413.97	/	73,239.23	15.855
5	550.00	20.72	1034.63	2.734	3099.68	529.77	/	84,301.17	14.260
6	433.11	7.40	906.74	2.763	3099.68	392.97	/	62,533.52	14.260
7	271.71	7.40	722.28	2.467	3099.68	296.85	/	47,237.39	14.260
8	132.69	7.40	564.63	2.133	3099.68	238.91	/	38,017.79	14.260
9	108.26	7.40	534.91	2.057	2309.66	231.72	/	27,475.03	14.260
10	50.00	7.40	447.38	1.806	2309.66	218.94	/	25,959.82	14.260
11	25.00	0.1013	104.92	0.367	2485.38	0.00	/	0.00	0.000
12	35.00	0.1013	146.72	0.505	2485.38	0.69	/	0.00	0.000
13	35.00	0.1013	146.72	0.505	1801.09	0.69	/	0.00	0.000

Table 11. *Cont.*

State Points	T	P	h	s	m	e_{ph}	e_{ch}	$\dot{C}$	c
	(°C)	(MPa)	(kJ/kg)	(kJ/(kg·K))	(kg/s)	(kJ/kg)	(kJ/kg)	($/h)	($/GJ)
14	29.00	0.1013	121.64	0.423	1801.09	0.11	/	0.00	0.000
A1	26.00	1.0345	1627.18	5.779	44.37	323.24	19,805.29	71,903.43	22.363
A2	55.00	1.0345	190.82	1.400	255.36	46.26	10,889.39	225,020.13	22.383
A3	55.27	2.3111	193.01	1.402	255.36	47.95	10,889.39	225,116.94	22.390
A4	93.26	2.3111	390.83	1.970	255.36	76.45	10,889.39	225,820.58	22.401
A5	60.47	1.0345	178.12	1.331	210.99	22.81	9014.33	153,708.18	22.393
A6	60.27	2.3111	178.12	1.327	210.99	24.21	9014.33	153,708.18	22.389
A7	110.00	2.3111	417.55	1.996	210.99	64.20	9014.33	154,388.21	22.389
A8	110.00	2.3111	1810.74	5.970	44.37	449.85	19,805.29	72,304.83	22.347
A9	55.00	2.3111	609.26	2.347	44.37	328.52	19,805.29	71,871.72	22.347
A10	26.00	1.0345	609.26	2.376	44.37	319.83	19,805.29	71,871.72	22.357
H1	45.00	1.00	189.30	0.638	3144.32	3.58	/	0.00	0.000
H2	49.65	1.00	208.72	0.699	3144.32	4.94	/	615.28	11.012
H3	53.70	1.00	225.67	0.751	3144.32	6.33	/	1060.68	14.807
H4	45.00	1.00	189.30	0.638	1903.60	3.58	/	0.00	0.000
H5	70.39	1.00	295.50	0.959	1903.60	14.03	/	1778.22	18.491
H6	60.00	1.00	252.00	0.831	5047.92	8.87	/	2838.90	17.614

Table 12 shows the thermodynamic properties and costs of exergy streams for the sCO_2/DH system.

Table 12. Thermodynamic properties and costs of exergy streams for the sCO_2/DH system.

State Points	T	P	h	s	e_{ph}	m	$\dot{C}$	c
	(°C)	(MPa)	(kJ/kg)	(kJ/(kg·K))	(kJ/kg)	(kg/s)	($/h)	($/GJ)
1	35.00	7.40	402.40	1.663	216.60	2309.66	26,014.53	14.445
2	110.06	20.72	444.87	1.680	254.09	2309.66	33,257.10	15.741
3	245.43	20.72	656.60	2.159	322.95	3099.68	57,527.04	15.963
4	393.02	20.72	841.06	2.473	413.97	3099.68	73,115.84	15.828
5	550.00	20.72	1034.63	2.734	529.77	3099.68	84,177.77	14.240
6	433.11	7.40	906.74	2.763	392.97	3099.68	62,441.98	14.240
7	271.71	7.40	722.28	2.467	296.85	3099.68	47,168.25	14.240
8	132.69	7.40	564.52	2.132	238.88	3099.68	37,957.41	14.240
10	50.00	7.40	447.38	1.806	218.94	2309.66	25,921.82	14.240
11	25.00	0.1013	104.92	0.367	0.00	8957.55	0.00	0.000
12	35.00	0.1013	146.72	0.505	0.00	8957.55	0.00	0.000
H4	45.00	1.0	189.30	0.638	3.58	4314.5	1775.3	31.890
H6	60.00	1.0	252.00	0.831	8.87	4314.5	4393.2	31.890

5.1. Parametric Analysis

The influences of several key parameters on the thermodynamic and exergoeconomic performances of the overall system are revealed through parametric analysis. The parameters studied include the turbine inlet temperature (T_5), the compressor pressure ratio (PRc), the generator outlet temperature (T_{A8}), and the evaporator outlet temperature (T_{A1}). As the turbine outlet pressure is set as 7.4 MPa to keep the sCO_2 topping cycle operating in the supercritical state, the PRc also represents the turbine inlet pressure. Both turbine inlet temperature and pressure are the vital parameters of sCO_2 topping cycle that can influence the electric power generation significantly, while other two parameters are important to the AHP bottoming cycle that can greatly affect the heat production. The parametric analysis is carried out by changing only one parameter at a time with all other parameters fixed.

5.1.1. Effects of the Compressor Pressure Ratio (PRc)

Figure 2 depicts the influences of PRc on the system performance indicators, namely COPP, COHP, exergy efficiency η_{ex} and total product unit cost c_{total}, for a single sCO_2 system, sCO_2/DH system, sCO_2/ammonia-water AHP system, and sCO_2/LiBr-H_2O AHP system, respectively. Obviously in Figure 2a, the thermodynamic and exergoeconomic performances for these four systems can be ranked according to η_{ex} and c_{total} as: sCO_2/LiBr-H_2O AHP > sCO_2/ammonia-water AHP > sCO_2/DH > sCO_2 (A > B means A is better than B). Thus, the combined cycles show better performances than the single sCO_2. This indicates that the performance of recompression sCO_2 cycle can be enhanced by assembling a waste heat recovery system based on the energy cascade utilization principle. Besides, by comparing three combined cycles, it can be concluded that AHP is a better choice than DH, and that the LiBr-H_2O solution is a better working fluid than the ammonia-water solution for AHP. Thus, the proposed sCO_2/LiBr-H_2O AHP system is a desirable waste heat recovery system for the sCO_2 cycle, with which the combined cycle could achieve a high exergy efficiency with a low cost.

Figure 2 shows the variation trends of system performance indicators with *PRc* for different thermal systems: (a) η_{ex} and c_{total}; (b) *COPP* and *COHP*.

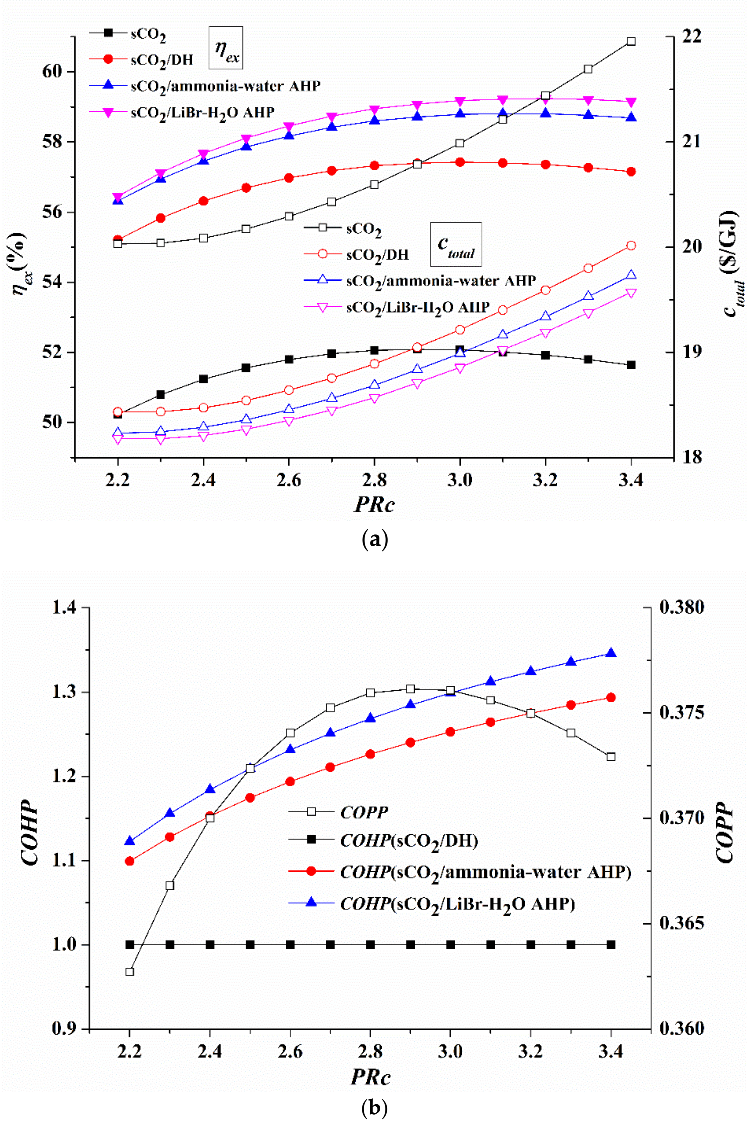

Figure 2. Variation trends of system performance indicators with *PRc* for different thermal systems: (**a**) η_{ex} and c_{total}; (**b**) *COPP* and *COHP*.

In Figure 2a, c_{total} increases with *PRc* due to the significant increments of capital investment, operation, and maintenance costs for the turbine, compressors and pressure vessels. Differently, η_{ex} increases firstly but then decreases with *PRc* in the research range, indicating the existence of an optimal *PRc* to maximize the exergy efficiency. As η_{ex} reflects the overall system performance considering both power generation and heat production, the above phenomenon can be analyzed and explained using these two aspects. Figure 2b depicts the variations of *COPP* and *COHP* with *PRc*. *COPP* represents the power generation capacity while *COHP* reflects the heat production capacity. Clearly, *COHP* increases with *PRc*, but *COPP* increases firstly and then decreases. Figure 3 presents the turbine output power $W_{\rm tur}$, compressor power consumption $W_{\rm com}$ and net output power $W_{\rm net}$ varying with *PRc* for the sCO_2/LiBr-H_2O AHP system. The increase of *PRc* (turbine inlet pressure) strengthens the power generation capacity of the unit mass working fluid, and leads to the increase of $W_{\rm tur}$. At the same time, the increase of the turbine inlet pressure requires more power to drive the compressors and leads to the increase of $W_{\rm com}$. So, with the increase of *PRc*, $W_{\rm net}$ increases firstly when the increment of $W_{\rm tur}$ is larger than that of $W_{\rm com}$, and then decreases for the opposite situation. It explains why *COPP* and η_{ex} increase firstly but then decrease with *PRc* in Figure 2a,b.

Figure 3 shows the variation trends of $W_{\rm tur}$, $W_{\rm com,}$ and $W_{\rm net}$ with *PRc* for the sCO_2/LiBr-H_2O AHP system.

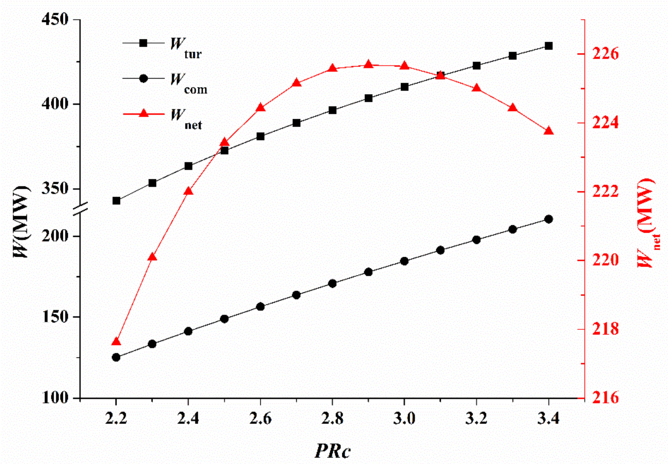

Figure 3. Variation trends of $W_{\rm tur}$, $W_{\rm com,}$ and $W_{\rm net}$ with *PRc* for the sCO_2/LiBr-H_2O AHP system.

5.1.2. Effects of the Turbine Inlet Temperature (T_5)

The effects of T_5 on η_{ex}, c_{total}, *COPP,* and *COHP* are displayed in Figure 4 for four thermal systems. Clearly, η_{ex} increases with T_5 while c_{total} shows an opposite variation trend. It indicates that increasing T_5 could be beneficial to the improvement of system performances for these thermal systems. Figure 5 depicts the net output power $W_{\rm net}$, the temperature of stream 8 (T_8) and the mass flow rate of 8a ($m_{8\rm a}$) varying with T_5 for the sCO_2/LiBr-H_2O AHP system. When T_5 ascends, the working capacity of unit mass working fluid is strengthened, and $W_{\rm net}$ increases correspondingly. As a result, *COPP* in Figure 4b also increases with T_5. On the other side, the increase of T_5 enlarges the heat absorption amount of the unit mass flow rate CO_2 from the reactor, so that the mass flow rate of CO_2 decreases. Correspondingly, $m_{8\rm a}$ decreases with the increase of T_5, as shown in Figure 5. It means that the mass flow rate of CO_2 flowing into AHP and DHE decreases, which in turn decreases the heat absorption amount of AHP and DHE from the topping cycle. At the same time, T_8 increases with T_5, so that the generator temperature ascends and the heat absorption amount of AHP and DHE from the topping cycle will increase. The opposite effects between T_8 and $m_{8\rm a}$ makes the *COHP* of sCO_2/AHP systems change slightly, as shown in Figure 4b. Thus, the increase of η_{ex} with T_5 is dominated by the increase of *COPP*, i.e., the power generation capacity of sCO_2 topping cycle, while the increase of T_5 exerts slight influences on the performances of the bottoming cycle. As the increase of T_5 results in the decrement of mass flow rate of working fluid, the capital investment costs for the turbine, compressors, and pressure vessels decrease correspondingly and lead to the decline of c_{total}, as shown in Figure 4a.

The following Figure 4 shows the variation trends of system performance indicators with T_5 for different thermal systems: (a) η_{ex} and c_{total}; (b) *COPP* and *COHP*.

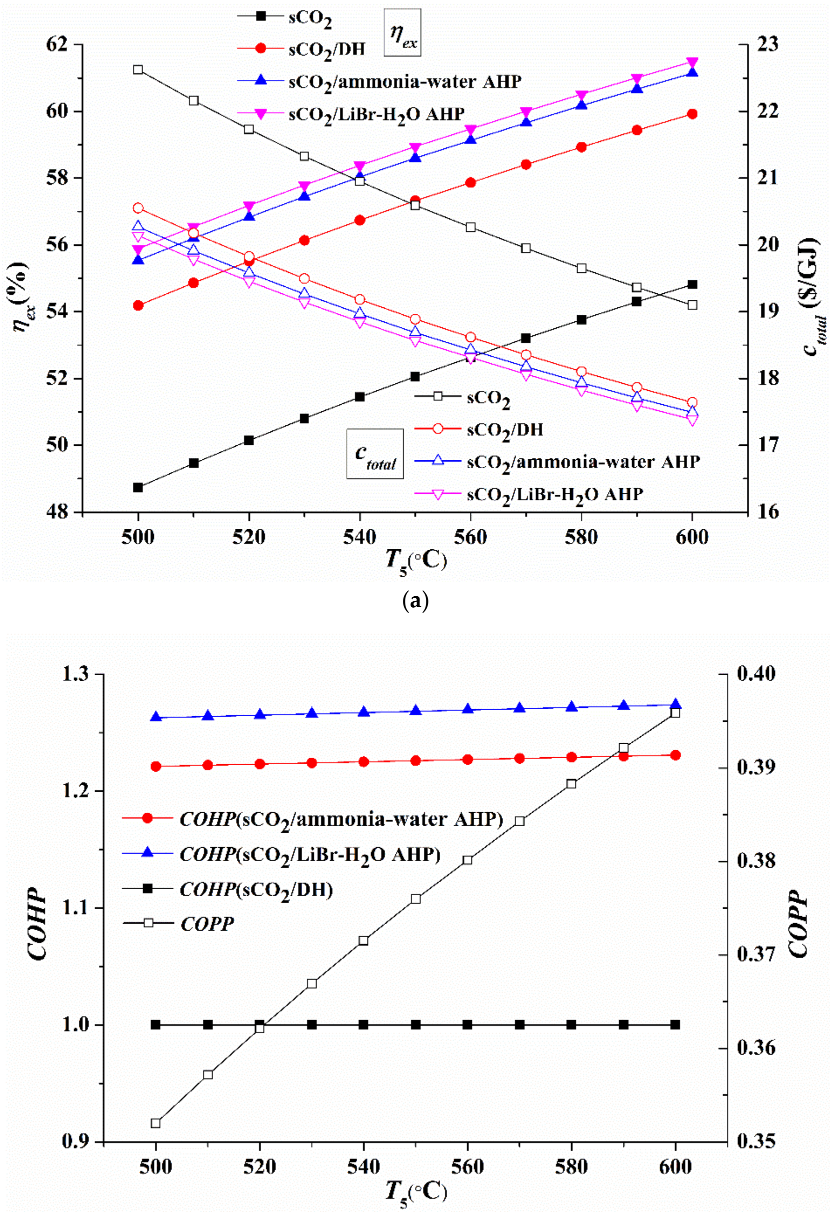

Figure 4. Variation trends of system performance indicators with T_5 for different thermal systems: (**a**) η_{ex} and c_{total}; (**b**) *COPP* and *COHP*.

The following Figure 5 shows the variation trends of T_8, m_{8a}, and W_{net} with T_5 for the sCO_2/LiBr-H_2O AHP system.

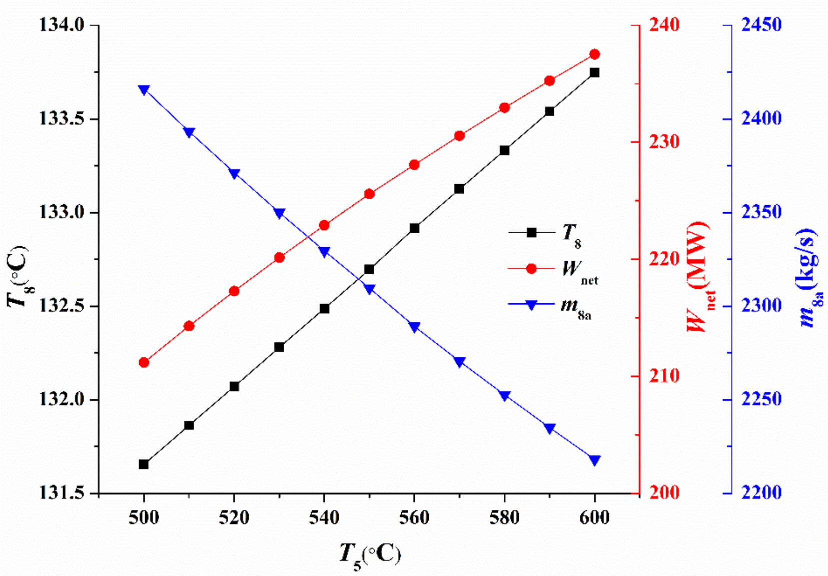

Figure 5. Variation trends of T_8, $m_{8a,}$ and W_{net} with T_5 for the sCO_2/LiBr-H_2O AHP system.

5.1.3. Effects of the Generator Outlet Temperature (T_{A8})

Then, the influences of key parameters of AHP bottoming cycle on the overall system performances are investigated. As the single sCO_2 cycle and the sCO_2/DH system have no AHP bottoming cycle, only the sCO_2/ammonia-water AHP system and the sCO_2/LiBr-H_2O AHP system are analyzed here. Figure 6 shows the variation of η_{ex} and c_{total} with the generator outlet temperature T_{A8} for these two combined systems. As T_{A8} increases, η_{ex} increases to a peak and next goes down slightly, while c_{total} shows an opposite trend in Figure 6a, which indicates that there exists a T_{A8} to optimize the overall system performances for the sCO_2/ammonia-water AHP system. The *COHP* also ascends firstly and then descends with T_{A8}. In order to explain this phenomenon, Figure 7a presents the mass flow rate of stream A8 (m_{A8}), the total mass flow rate of ammonia water (m_{A4}), the pump power consumption (W_{pump}), and the exergy that heat users obtain ($E_{h,users}$) varying with T_{A8}. Clearly, as T_{A8} increases, the heat absorption amount per unit mass flow rate from the topping cycle increases, so that the total mass flow rate m_{A4} descends and then leads to the decline of W_{pump}. m_{A8} increases firstly with T_{A8} as more working fluid is evaporated from the generator solution. More ammonia vapor flows into the condenser and releases the considerable latent heat to the heating water, so that $E_{h,users}$ increases correspondingly. Then, as the effect of decreasing m_{A4} dominates when T_{A8} is larger, both m_{A8} and $E_{h,users}$ decrease with T_{A8}. Therefore, *COHP* and η_{ex} increase and then decrease with T_{A8} according to Equations (41) and (42).

Figure 6 shows the variation trends of η_{ex}, c_{total}, and *COHP* with T_{A8}: (a) a sCO_2/ammonia-water AHP system; (b) a sCO_2/LiBr-H_2O AHP system.

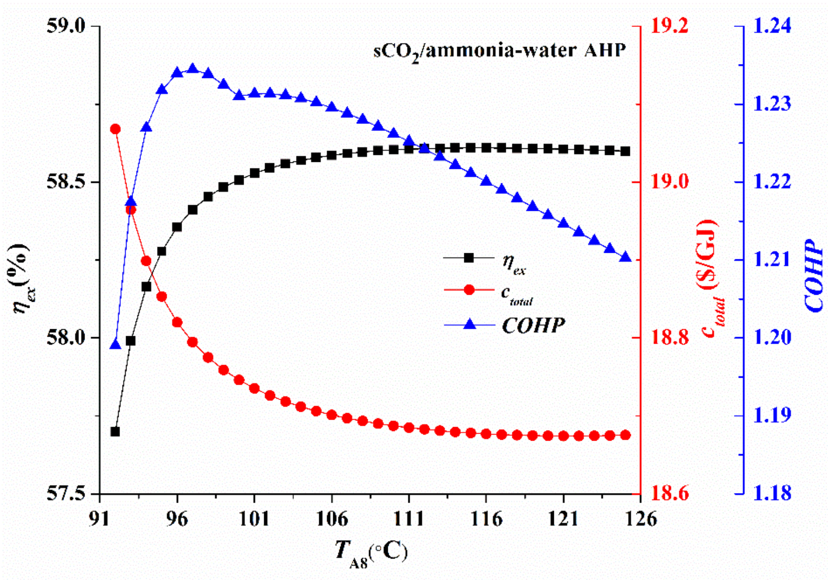

(**a**)

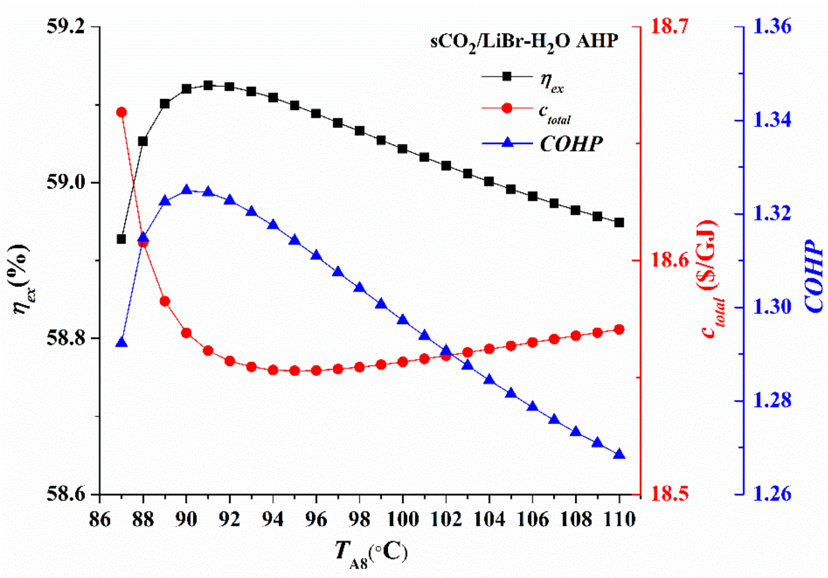

(**b**)

Figure 6. Variation trends of η_{ex}, c_{total} and *COHP* with T_{A8}: (**a**) sCO_2/ammonia-water AHP system; (**b**) sCO_2/LiBr-H_2O AHP system.

The following Figure 7 shows the variation trends of m_{A8}, m_{A4}, W_{pump}, and $E_{h,users}$ with T_{A8}: (a) a sCO_2/ammonia-water AHP system; (b) a sCO_2/LiBr-H_2O AHP system.

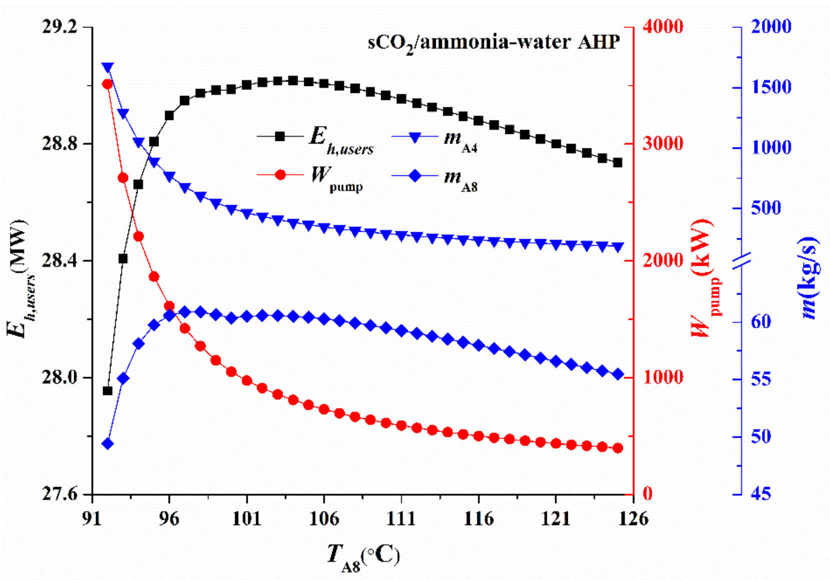

(**a**)

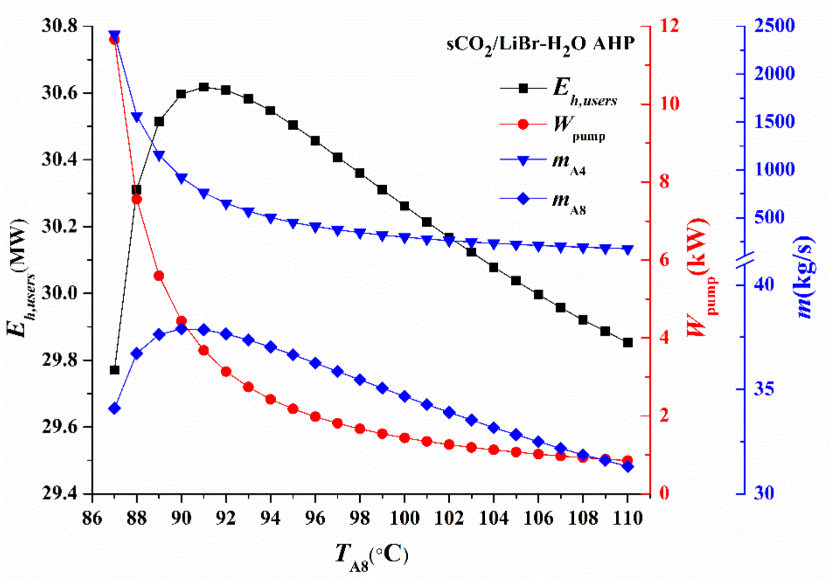

(**b**)

Figure 7. Variation trends of m_{A8}, m_{A4}, W_{pump}, and $E_{h,users}$ with T_{A8}: (**a**) a sCO_2/ammonia-water AHP system; (**b**) a sCO_2/LiBr-H_2O AHP system.

For the sCO_2/LiBr-H_2O AHP system, the same trends can be observed for the *COHP*, m_{A4}, m_{A8}, W_{pump}, and $E_{h,users}$ in Figures 6b and 7b, which will not be explained again here. It should be noted that the operational pressure of LiBr-H_2O AHP is much lower than that of ammonia-water AHP, so the pump power consumption W_{pump} in LiBr-H_2O AHP is also lower than that in ammonia-water AHP, as shown in Figure 7.

5.1.4. Effects of the Evaporator Temperature (T_{A1})

Figure 8 describes the variations of η_{ex}, c_{total} and *COHP* with T_{A1}. When T_{A1} increases, more heat is transferred to the heating water in the absorber. The heat absorption amount of heating water ascends correspondingly, and results in the increase of *COHP*. As the pump work is very limited compared to the turbine output power, the variation of pump power consumption with T_{A1} has ignorable effects on the net output power. Thus, the power generation capacity is hardly affected by the change of T_{A1}. This means that the overall system performances are mainly affected by the variation of heat production capacity when T_{A1} changes. Therefore, the exergy efficiency η_{ex} has the same variation trend of *COHP* and the total product unit cost c_{total} decreases with T_{A1}, indicating that the thermodynamic and economic performances of the sCO_2/AHP systems can be improved by increasing the evaporator temperature.

The following Figure 8 shows the variation trends of system performance indicators with T_{A1} for different thermal systems: (a) η_{ex} and c_{total}; (b) *COHP*.

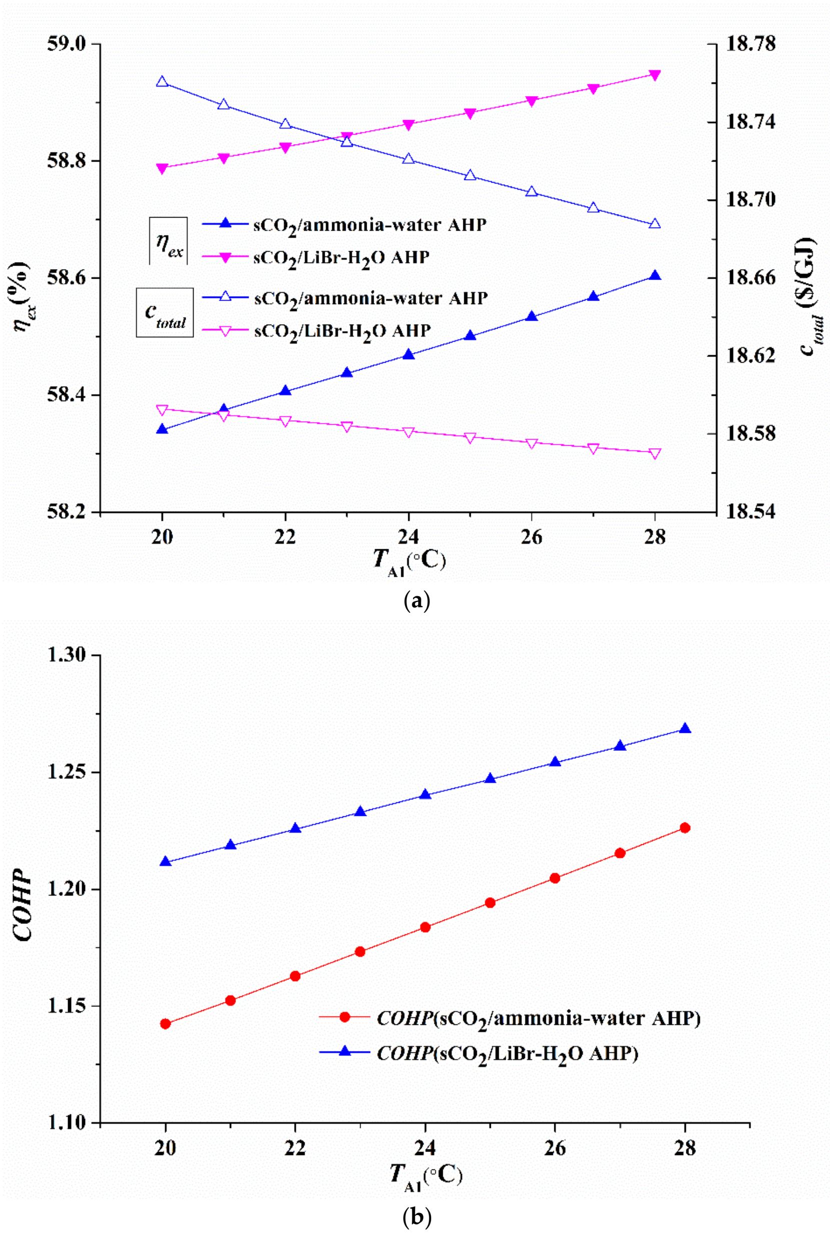

Figure 8. Variation trends of system performance indicators with T_{A1} for different thermal systems: (**a**) η_{ex} and c_{total}; (**b**) *COHP*.

5.2. System Performance Optimization and Comparison

Finally, parameter optimizations are carried out in this section to provide references for the practical design and operation. The overall performances of a single sCO_2 system, sCO_2/DH system, sCO_2/ammonia-water AHP system and sCO_2/LiBr-H_2O AHP system are optimized by using the particle swarm optimization (PSO) algorithm, which was proposed by Kennedy and Eberhart [54]. The PSO algorithm shows higher accuracy and converges faster compared to other optimization algorithms, and has been successfully applied to optimize performances for thermal systems [55,56]. A swarm of particles is included in the PSO algorithm to represent the candidate solutions. Each candidate solution has a velocity vector $\vec{v}$ and a position vector $\vec{u}$. In addition, a best global position $\vec{g}(t)$ and a best personal position $\vec{p}(t)$ are stored for each particle. For each time step t, the particles move to a better position in the space so that the velocity vector $\vec{v}$ and the position vector $\vec{u}$ update correspondingly, as shown in Equations (46) and (47):

$$\vec{u}(t+1) = \vec{u}(t) + \vec{v}(t+1) \tag{46}$$

$$\vec{v}(t+1) = \varpi\vec{v}(t) + U(0,\varphi_1)\left(\vec{p}(t) - \vec{u}(t)\right) + U(0,\varphi_2)\left(\vec{g}(t) - \vec{u}(t)\right) \tag{47}$$

where ϕ_1 and ϕ_2 denote the importance of $\vec{p}(t)$ and $\vec{g}(t)$, respectively. ϖ is the inertia weight that controls the velocity $\vec{v}(t)$.

In this study, the key parameters studied include the compressor pressure ratio PRc, the turbine inlet temperature T_5, the generator outlet temperature T_{A8}, and the evaporator temperature T_{A1}. The constraints of key parameters for the PSO algorithm are displayed in Table 13. The exergy efficiency η_{ex} and the total product unit cost c_{total} are chosen as the objective functions. The optimization is achieved by maximizing η_{ex} or minimizing c_{total}. So two optimal design cases are considered, namely, the exergy efficiency optimal design (EOD) case and the cost optimal design (COD) case. The inertia weight ϖ and the swarm size for the PSO algorithm are chosen as 0.6 and 25, respectively. Both ϕ_1 and ϕ_2 are chosen as 1.8. In addition, a maximal velocity v_{max} of 15% is adopted to constrain the velocity at each time step [57].

The following Table 13 shows the boundary conditions of decision variables for the PSO algorithm.

Table 13. Boundary conditions of decision variables for the PSO algorithm.

Items	sCO_2	sCO_2/DH	sCO_2/Ammonia-Water AHP	sCO_2/LiBr-H_2O AHP
PRc	2.2–3.3	2.2–3.3	2.2–3.3	2.2–3.3
T_5 (°C)	500–600	500–600	500–600	500–600
T_{A8} (°C)	/	/	92–125	87–110
T_{A1} (°C)	/	/	23–28	23–28

Tables 14 and 15 show the optimized results of these four thermal systems for the EOD case and the COD case, respectively. Obviously, due to the different optimization targets, the exergy efficiencies η_{ex} for the EOD case are much higher than those for the COD case, while the total product unit costs c_{total} for the COD case are lower than those for the EOD case. The optimum PRc for the COD case is smaller than that for the EOD case, meaning that the capital investment, operation, and maintenance costs for the turbine, compressors and pressure vessels are lower, which leads to a lower c_{total} in the COD case. The total product unit costs c_{total} of a sCO_2 system, sCO_2/DH system, sCO_2/ammonia-water AHP system, and sCO_2/LiBr-H_2O AHP system for the COD case are about 4.00%, 4.39%, 4.39%, and 3.87% lower than those for the EOD case. As for the expense, the exergy efficiencies η_{ex} of sCO_2 system, sCO_2/DH system, sCO_2/ammonia-water AHP system, and sCO_2/LiBr-H_2O AHP system for the COD case dropped by about 3.14%, 3.35%, 4.09%, and 4.13%, respectively. In both the COD case and the EOD case, the sCO_2/LiBr-H_2O AHP system has the highest η_{ex} with a lowest cost c_{total}, indicating that the overall system performances are greatly improved by combining the LiBr-H_2O AHP with sCO_2 cycle. In the the EOD case, η_{ex} of sCO_2/LiBr-H_2O AHP system is 13.39%, 3.53% and 1.13% higher than those of the sCO_2 system, sCO_2/DH system, and sCO_2/ammonia-water AHP system, respectively. In the the COD case, c_{total} of sCO_2/LiBr-H_2O AHP system is 8.66%, 1.27%, and 0.42% lower than those of sCO_2 system, sCO_2/DH system and sCO_2/ammonia-water AHP system, respectively. In addition, the *COHP* of the sCO_2/LiBr-H_2O AHP system is much larger than those of the sCO_2/DH system and the sCO_2/ammonia-water AHP system. It indicates that the LiBr-H_2O AHP can maximize the recovery of waste heat from sCO_2 cycle to provide heat for users.

Table 14 shows the optimized results for the exergy efficiency optimal design case.

Table 14. Optimized results for the exergy efficiency optimal design case.

Items	sCO_2	sCO_2/DH	sCO_2/Ammonia-Water AHP	sCO_2/LiBr-H_2O AHP
PRc	3.1641	3.2599	3.2960	3.2803
T_5 (°C)	600	600	600	599.31
T_{A8} (°C)	/	/	115.86	90.30
T_{A1} (°C)	/	/	28	27.92
COPP	0.3980	0.3979	0.3978	0.3975
COHP	/	1	1.282	1.410
η_{ex} (%)	55.11	60.36	61.79	62.49
c_{total} ($/GJ)	19.603	18.210	18.054	17.881

Table 15 shows the optimized results for the cost optimal design case.

Table 15. Optimized results for the cost optimal design case.

Items	sCO_2	sCO_2/DH	sCO_2/Ammonia-Water AHP	sCO_2/LiBr-H_2O AHP
PRc	2.3693	2.3692	2.3449	2.3992
T_5 (°C)	600	600	600	600
T_{A8} (°C)	/	/	114.31	96.98
T_{A1} (°C)	/	/	28	28
COPP	0.3855	0.3855	0.3845	0.3866
COHP	/	1	1.131	1.235
η_{ex} (%)	53.38	58.34	59.26	59.91
c_{total} ($/GJ)	18.819	17.410	17.262	17.189

6. Conclusions

In this study, a novel combined sCO_2/LiBr-H_2O AHP system is first proposed and analyzed for heat and power cogeneration according to the principle of energy cascade utilization. Detailed thermodynamic and exergoeconomic analysis, parametric studies, optimizations, and comparisons are carried out among a stand-alone sCO_2 system, a sCO_2/DH system, a sCO_2/ammonia-water AHP system, and the proposed sCO_2/LiBr-H_2O AHP system. The main conclusions and contributions of this work can be summarized as follows:

1. Using the LiBr-H_2O AHP to recover the waste heat from sCO_2 cycle can significantly improve the thermodynamic and economic performances for the overall system. Based on the optimization results, the sCO_2/LiBr-H_2O AHP system can gain an improvement of 13.39% in the exergy efficiency and a reduction of 8.66% in the total product unit cost compared to the stand-alone sCO_2 cycle;
2. The exergy efficiency of sCO_2/LiBr-H_2O AHP system is 3.53% and 1.13% higher than those of sCO_2/DH system and sCO_2/ammonia-water AHP system, respectively, in the EOD case, and the total product unit cost of the sCO_2/LiBr-H_2O AHP system is 1.27% and 0.42% lower than those of the sCO_2/DH system and sCO_2/ammonia-water AHP system, respectively in the the COD case. In addition, *COHP* of sCO_2/LiBr-H_2O AHP system is much larger than those of sCO_2/DH system and sCO_2/ammonia-water AHP system, indicating that the LiBr-H_2O AHP can maximize the recovery of waste heat from sCO_2 cycle to provide heat for users. Therefore, the LiBr-H_2O AHP is a desirable waste heat recovery system for the sCO_2 cycle, with which the combined system could achieve a higher exergy efficiency and a lower cost. Besides, the proposed sCO_2/LiBr-H_2O

AHP system is presented to be a high-efficiency CHP system. It provides a meaningful direction for the design and improvement of sCO_2-based CHP systems to reduce energy consumption and to bring considerable economic benefits;

3. The parametric study presents the influences of decision variables on the system performances, and the PSO optimization finds optimal design conditions for different cases. The results of parametric study, optimization, and comparison analysis could provide useful references for designers and researchers attempting to obtain desirable system designs and operation conditions for sCO_2-based CHP systems.

Author Contributions: Conceptualization, methodology, data curation, writing—original draft preparation, visualization, Y.Y.; software, validation, investigation, Z.W., Q.M. and Y.L.; investigation, writing—review and editing, J.W. and P.Z.; supervision, Y.D. All authors have read and agreed to the published version of the manuscript.

Funding: This research is support by the State Key Special Research Project of the Ministry of Science and Technology of China (Grant No. 2017YFB0603504 and No. 2016YFB0600104), and the National Natural Science Foundation of China (Grant No. 51976145 and No. 51976147).

Acknowledgments: The authors would like to sincerely thank all the reviewers for the valuable comments that greatly helped to improve the manuscript. Yi Yang wants to acknowledge the technical support from Hang Li from Zhengzhou University.

Conflicts of Interest: The authors declare no conflict of interest.

Nomenclature

A	heat transfer area (m^2)
$\dot{C}$	cost rate ($/h)
c	cost per unit exergy ($/GJ)
c_{total}	total product unit cost ($/GJ)
e	specific exergy (kJ/kg)
E	exergy rate (kW)
h	enthalpy (kJ/kg)
i_r	interest rate
I	exergy destruction (kW)
m	mass flow rate (kg/s)
n	number of operation year
P	pressure (MPa)
PRc	compressor pressure ratio
Q	heat transfer rate (kW)
s	entropy (kJ/(kg·K))
T	temperature (°C)
W	power (kW)
x	recompressed mass flow ratio
y	concentration of LiBr or ammonia in the solution
Z	capital cost of a component ($)
$\dot{Z}$	capital cost rate ($/h)
Greek letters	
η	efficiency (%)
ε	effectiveness
γ	maintenance factor
τ	annual operation hours (h)
Subscripts and abbreviations	
0	ambient state
1, 2, et al.	state points
A	state points of absorption heat pump
AHP	absorption heat pump
Abs	absorber

ch	chemical exergy
CI	capital investment
COD	cost optimal design
com	compressor
Cond	condenser
COHP	coefficient of heat performance
COPP	coefficient of power performance
core	reactor core
CRF	capital recovery factor
DH	direct heating
DHE	direct heating exchanger
EOD	exergy efficiency optimal design
ex	exergy
Eva	evaporator
Gen	generator
H	state points of heating water
HTR	high temperature recuperator
LTR	low temperature recuperator
LMTD	logic mean temperature difference
MC	main compressor
mcom	main compressor
OM	operation and maintenance
ph	physical exergy
pump	pump
RC	recompression compressor
rcom	recompression compressor
SHE	solution heat exchanger
tur	turbine

References

1. Liao, G.; Liu, L.; Jiaqiang, E.; Zhang, F.; Chen, J.; Deng, Y.; Zhu, H. Effects of technical progress on performance and application of supercritical carbon dioxide power cycle: A review. *Energy Convers. Manag.* **2019**, *199*, 111986. [CrossRef]
2. Li, M.; Zhu, H.; Guo, J.; Wang, K.; Tao, W. The development technology and applications of supercritical co2 power cycle in nuclear energy, solar energy and other energy industries. *Appl. Therm. Eng.* **2017**, *126*, 255–275. [CrossRef]
3. Crespi, F.; Gavagnin, G.; Sánchez, D.; Martínez, G.S. Supercritical carbon dioxide cycles for power generation: A review. *Appl. Energy* **2017**, *195*, 152–183. [CrossRef]
4. Ahn, Y.; Bae, S.J.; Kim, M.; Cho, S.K.; Baik, S.; Lee, J.I.; Cha, J.E. Review of supercritical co2 power cycle technology and current status of research and development. *Nucl. Eng. Technol.* **2015**, *47*, 647–661. [CrossRef]
5. Sarkar, J. Second law analysis of supercritical co2 recompression brayton cycle. *Energy* **2009**, *34*, 1172–1178. [CrossRef]
6. Sarkar, J.; Bhattacharyya, S. Optimization of recompression S-CO_2 power cycle with reheating. *Energy Convers. Manag.* **2009**, *50*, 1939–1945. [CrossRef]
7. Wang, X.; Yang, Y.; Zheng, Y.; Dai, Y. Exergy and exergoeconomic analyses of a supercritical co2 cycle for a cogeneration application. *Energy* **2017**, *119*, 971–982. [CrossRef]
8. Yari, M.; Sirousazar, M. A novel recompression s-co2 brayton cycle with pre-cooler exergy utilization. *Proc. Inst. Mech. Eng. Part A J. Power Energy* **2010**, *224*, 931–946. [CrossRef]
9. Pérez-Pichel, G.D.; Linares, J.; Herranz, L.; Moratilla, B. Thermal analysis of supercritical co2 power cycles: Assessment of their suitability to the forthcoming sodium fast reactors. *Nucl. Eng. Des.* **2012**, *250*, 23–34. [CrossRef]
10. Chacartegui, R.; De Escalona, J.M.; Sánchez, D.; Monje, B.; Sánchez, T. Alternative cycles based on carbon dioxide for central receiver solar power plants. *Appl. Therm. Eng.* **2011**, *31*, 872–879. [CrossRef]

11. Akbari, A.D.; Mahmoudi, S.M. Thermoeconomic analysis & optimization of the combined supercritical co2 (carbon dioxide) recompression brayton/organic rankine cycle. *Energy* **2014**, *78*, 501–512.
12. Wang, X.; Dai, Y. Exergoeconomic analysis of utilizing the transcritical CO_2 cycle and the orc for a recompression supercritical CO_2 cycle waste heat recovery: A comparative study. *Appl. Energy* **2016**, *170*, 193–207. [CrossRef]
13. Besarati, S.M.; Goswami, D.Y. Analysis of advanced supercritical carbon dioxide power cycles with a bottoming cycle for concentrating solar power applications. *J. Sol. Energy Eng.* **2014**, *136*, 010904. [CrossRef]
14. Li, H.; Wang, M.; Wang, J.; Dai, Y. Exergoeconomic analysis and optimization of a supercritical CO_2 cycle coupled with a kalina cycle. *J. Energy Eng.* **2016**, *143*, 04016055. [CrossRef]
15. S Mahmoudi, S.; D Akbari, A.; Rosen, M. Thermoeconomic analysis and optimization of a new combined supercritical carbon dioxide recompression brayton/kalina cycle. *Sustainability* **2016**, *8*, 1079. [CrossRef]
16. Hu, B.; Li, Y.; Wang, R.; Cao, F.; Xing, Z. Real-time minimization of power consumption for air-source transcritical co2 heat pump water heater system. *Int. J. Refrig.* **2018**, *85*, 395–408. [CrossRef]
17. Wu, C.; Wang, S.-S.; Feng, X.-J.; Li, J. Energy, exergy and exergoeconomic analyses of a combined supercritical co2 recompression brayton/absorption refrigeration cycle. *Energy Convers. Manag.* **2017**, *148*, 360–377. [CrossRef]
18. Li, H.; Su, W.; Cao, L.; Chang, F.; Xia, W.; Dai, Y. Preliminary conceptual design and thermodynamic comparative study on vapor absorption refrigeration cycles integrated with a supercritical co2 power cycle. *Energy Convers. Manag.* **2018**, *161*, 162–171. [CrossRef]
19. Balafkandeh, S.; Zare, V.; Gholamian, E. Multi-objective optimization of a tri-generation system based on biomass gasification/digestion combined with S-CO_2 cycle and absorption chiller. *Energy Convers. Manag.* **2019**, *200*, 112057. [CrossRef]
20. Zhang, X.; Yamaguchi, H.; Fujima, K.; Enomoto, M.; Sawada, N. Theoretical analysis of a thermodynamic cycle for power and heat production using supercritical carbon dioxide. *Energy* **2007**, *32*, 591–599. [CrossRef]
21. Moroz, L.; Burlaka, M.; Rudenko, O. Study of a supercritical CO2 power cycle application in a cogeneration power plant. In Proceedings of the 5th Supercritical CO2 Power Cycles Symposium, San Antonio, TX, USA, 28–31 March 2016.
22. Xu, Z.; Wang, R. Absorption heat pump for waste heat reuse: Current states and future development. *Front. Energy* **2017**, *11*, 414–436. [CrossRef]
23. Hassan, H.; Mohamad, A. A review on solar cold production through absorption technology. *Renew. Sustain. Energy Rev.* **2012**, *16*, 5331–5348. [CrossRef]
24. Horuz, I. A comparison between ammonia-water and water-lithium bromide solutions in vapor absorption refrigeration systems. *Int. Commun. Heat Mass Transf.* **1998**, *25*, 711–721. [CrossRef]
25. Jia, T.; Dai, Y. Development of a novel unbalanced ammonia-water absorption-resorption heat pump cycle for space heating. *Energy* **2018**, *161*, 251–265. [CrossRef]
26. Moran, M.J.; Shapiro, H.N.; Boettner, D.D.; Bailey, M.B. *Fundamentals of Engineering Thermodynamics*; John Wiley & Sons: Hoboken, NJ, USA, 2010.
27. Herold, K.E.; Radermacher, R.; Klein, S.A. *Absorption Chillers and Heat Pump*; CRC press: Lancaster, PA, USA, 2016.
28. Sun, D.-W. Comparison of the performances of nh3-h2o, nh3-lino3 and nh3-nascn absorption refrigeration systems. *Energy Convers. Manag.* **1998**, *39*, 357–368. [CrossRef]
29. Zare, V.; Mahmoudi, S.; Yari, M. On the exergoeconomic assessment of employing kalina cycle for gt-mhr waste heat utilization. *Energy Convers. Manag.* **2015**, *90*, 364–374. [CrossRef]
30. Misra, R.; Sahoo, P.; Gupta, A. Thermoeconomic evaluation and optimization of an aqua-ammonia vapour-absorption refrigeration system. *Int. J. Refrig.* **2006**, *29*, 47–59. [CrossRef]
31. Palacios-Bereche, R.; Gonzales, R.; Nebra, S.A. Exergy calculation of lithium bromide-water solution and its application in the exergetic evaluation of absorption refrigeration systems libr-h2o. *Int. J. Energy Res.* **2012**, *36*, 166–181. [CrossRef]
32. Bejan, A.; Tsatsaronis, G.; Moran, M. *Thermal Design and Optimization*; John Wiley & Sons: Hoboken, NJ, USA, 1995.

33. Ghaebi, H.; Amidpour, M.; Karimkashi, S.; Rezayan, O. Energy, exergy and thermoeconomic analysis of a combined cooling, heating and power (cchp) system with gas turbine prime mover. *Int. J. Energy Res.* **2011**, *35*, 697–709. [CrossRef]
34. Farshi, L.G.; Mahmoudi, S.S.; Rosen, M.; Yari, M.; Amidpour, M. Exergoeconomic analysis of double effect absorption refrigeration systems. *Energy Convers. Manag.* **2013**, *65*, 13–25. [CrossRef]
35. Carstens, N.; Hejzlar, P.; Driscoll, M.J. *Control System Strategies and Dynamic Response for Supercritical CO2 Power Conversion Cycles*; Report No. MIT-GFR-038; Center for Advanced Nuclear Energy Systems, MIT Nuclear Engineering Department: Cambridge, MA, USA, 2006.
36. Nikitin, K.; Kato, Y.; Ngo, L. Printed circuit heat exchanger thermal–hydraulic performance in supercritical co2 experimental loop. *Int. J. Refrig.* **2006**, *29*, 807–814. [CrossRef]
37. Meshram, A.; Jaiswal, A.K.; Khivsara, S.D.; Ortega, J.D.; Ho, C.; Bapat, R.; Dutta, P. Modeling and analysis of a printed circuit heat exchanger for supercritical co2 power cycle applications. *Appl. Therm. Eng.* **2016**, *109*, 861–870. [CrossRef]
38. Serrano, I.; Cantizano, A.; Linares, J.; Moratilla, B. Modeling and sizing of the heat exchangers of a new supercritical co2 brayton power cycle for energy conversion for fusion reactors. *Fusion Eng. Des.* **2014**, *89*, 1905–1908. [CrossRef]
39. Li, H.; Yang, Y.; Cheng, Z.; Sang, Y.; Dai, Y. Study on off-design performance of transcritical CO_2 power cycle for the utilization of geothermal energy. *Geothermics* **2018**, *71*, 369–379. [CrossRef]
40. Cayer, E.; Galanis, N.; Desilets, M.; Nesreddine, H.; Roy, P. Analysis of a carbon dioxide transcritical power cycle using a low temperature source. *Appl. Energy* **2009**, *86*, 1055–1063. [CrossRef]
41. Yin, H. An Absorption Chiller in a Micro Bchp Application: Model Based Design and Performance Analysis. Ph.D. Thesis, Carnegie Mellon University, Pittsburgh, PA, USA, 2006.
42. Táboas, F.; Valles, M.; Bourouis, M.; Coronas, A. Pool boiling of ammonia/water and its pure components: Comparison of experimental data in the literature with the predictions of standard correlations. *Int. J. Refrig.* **2007**, *30*, 778–788. [CrossRef]
43. Kreith, F.; Manglik, R.M.; Bohn, M.S. *Principles of Heat Transfer*; Cengage learning: Stamford, CT, USA, 2012.
44. Florides, G.A.; Kalogirou, S.A.; Tassou, S.A.; Wrobel, L.C. Design and construction of a libr–water absorption machine. *Energy Convers. Manag.* **2003**, *44*, 2483–2508. [CrossRef]
45. Lee, S. *Development of Techniques for In-Situ Measurement of Heat and Mass Transfer in Ammonia-Water Absorption Systems*; Georgia Institute of Technology: Atlanta, GA, USA, 2007.
46. Cengel, Y.A. *Heat Transfer: A Practical Approach*, 2nd ed.; McGraw Hill: New York, NY, USA, 2003.
47. Cheng, C.S.; Shih, Y.S. Exergy and energy analyses of absorption heat pumps. *Int. J. Energy Res.* **1988**, *12*, 189–203. [CrossRef]
48. Patek, J.; Klomfar, J. A computationally effective formulation of the thermodynamic properties of libr–h2o solutions from 273 to 500 k over full composition range. *Int. J. Refrig.* **2006**, *29*, 566–578. [CrossRef]
49. Boryta, D.A. Solubility of lithium bromide in water between-50. Deg. And+ 100. Deg.(45 to 70% lithium bromide). *J. Chem. Eng. Data* **1970**, *15*, 142–144. [CrossRef]
50. Wang, M.; Ferreira, C.A.I. Absorption heat pump cycles with nh3–ionic liquid working pairs. *Appl. Energy* **2017**, *204*, 819–830. [CrossRef]
51. Mohammadi, Z.; Fallah, M.; Mahmoudi, S.S. Advanced exergy analysis of recompression supercritical CO_2 cycle. *Energy* **2019**, *178*, 631–643. [CrossRef]
52. Shi, D.; Zhang, L.; Xie, Y.; Zhang, D. Aerodynamic design and off-design performance analysis of a multi-stage s-CO_2 axial turbine based on solar power generation system. *Appl. Sci.* **2019**, *9*, 714. [CrossRef]
53. Sun, J.; Fu, L.; Zhang, S. Experimental study of heat exchanger basing on absorption cycle for chp system. *Appl. Therm. Eng.* **2016**, *102*, 1280–1286. [CrossRef]
54. Kennedy, J.; Eberhart, R. Particle Swarm Optimization. In Proceedings of the IEEE international conference on neural networks, Perth, Australia, 27 November–1 December 1995; IEEE: Piscataway, NJ, USA, 1995; pp. 1942–1948.
55. Du, Y.; Yang, Y.; Hu, D.; Hao, M.; Wang, J.; Dai, Y. Off-design performance comparative analysis between basic and parallel dual-pressure organic rankine cycles using radial inflow turbines. *Appl. Therm. Eng.* **2018**, *138*, 18–34. [CrossRef]

56. Du, Y.; Chen, K.; Dai, Y. A study of the optimal control approach for a kalina cycle system using a radial-inflow turbine with variable nozzles at off-design conditions. *Appl. Therm. Eng.* **2019**, *149*, 1008–1022. [CrossRef]
57. Vesterstrom, J.; Thomsen, R. A comparative study of differential evolution, particle swarm optimization, and evolutionary algorithms on numerical benchmark problems. In Proceedings of the 2004 Congress on Evolutionary Computation, Portland, OR, USA, 19–23 June 2004; IEEE: New York, NY, USA, 2004; pp. 1980–1987.

© 2020 by the authors. Licensee MDPI, Basel, Switzerland. This article is an open access article distributed under the terms and conditions of the Creative Commons Attribution (CC BY) license (http://creativecommons.org/licenses/by/4.0/).